Regional-scale transport of air pollutants: Impacts of southern California emissions on Phoenix ground-level ozone concentrations

J. Li[1*], M. Georgescu[1,2,], P. Hyde[3], A. Mahalov[1], and M. Moustaoui[1]

[1] Julie Ann Wrigley Global Institute of Sustainability, School of Mathematical and Statistical Sciences, Arizona State University, Tempe, AZ 85287, USA

[2] School of Geographical Sciences and Urban Planning, Arizona State University, Tempe, AZ 85287, USA

[3] School for Engineering of Matter, Transport and Energy, Arizona State University, Tempe, AZ 85287, USA

[*]**Corresponding Author**: Jialun.Li@asu.edu

Revised manuscript submitted to *Atmospheric Chemistry and Physics(D)*

May, 2015

Abstract

In this study, WRF-Chem is utilized at high-resolution (1.333-km grid spacing for the innermost domain) to investigate impacts of southern California anthropogenic emissions (SoCal) on Phoenix ground-level ozone concentrations ([O_3]) for a pair of recent exceedance episodes. First, WRF-Chem control simulations, based on the U.S. Environmental Protection Agency (EPA) 2005 National Emissions Inventories (NEI05), are conducted to evaluate model performance. Compared with surface observations of hourly ozone, CO, NO_X, and wind fields, the Control simulations reproduce observed variability well. Simulated [O_3] are comparable with the previous studies in this region. Next, the relative contribution of SoCal and Arizona local anthropogenic emissions (AZ) to ozone exceedances within the Phoenix metropolitan area is investigated via a trio of sensitivity simulations: (1) SoCal emissions are excluded, with all other emissions as in Control; (2) AZ emissions are excluded with all other emissions as in Control; and (3) SoCal and AZ emissions are excluded (i.e., all anthropogenic emissions are eliminated) to account only for biogenic emissions [BEO]. Based on the USEPA NEI05, results for the selected events indicate the impacts of AZ emissions are dominant on daily maximum 8 h average (DMA8) [O_3] in Phoenix. SoCal contributions to DMA8 [O_3] for the Phoenix metropolitan area range from a few ppbv to over 30 ppbv (10%-30% relative to Control experiments). [O_3] from SoCal and AZ emissions exhibit the expected diurnal characteristics that are determined by physical and photochemical processes, while BEO contributions to DMA8 [O_3] in Phoenix also play a key role.

Finally, ozone transport processes and pathways within the lower troposphere are investigated. During daytime, pollutants (mainly ozone) near the southern California coasts are pumped into the planetary boundary-layer over the southern California desert through the

mountain chimney and pass channel effects, aiding eastward transport along the desert air basins in southern California and finally, northeastward along the lower Gila River basin in Arizona, thereby affecting Phoenix air quality during subsequent days. This study indicates that local emission controls in Phoenix need to be augmented with regional emission reductions to attain the federal ozone standard, especially if a more stringent standard is adopted in the future.

1. **Introduction**

Tropospheric ozone is a strong oxidant controlling much of the chemistry in the atmosphere, such as hydroxyl radical production and the lifetime of atmospheric species (see review in He et al., 2013). Tropospheric ozone is also a greenhouse gas and acts as a potent anthropogenic contributor to radiative forcing of climate (IPCC, 2007). Lower tropospheric ozone adversely affects human health (Anderson, 2009; Smith et al., 2009), reduces crop yields (Avnery et al., 2011; Chameides et al., 1999), and damages natural ecosystems (Ashmore, 2005; Mauzeral and Wang, 2001). Therefore, ozone (O_3) is one of the six criteria pollutants regulated by the US Environmental Protection Agency (EPA) through National Ambient Air Quality Standards (NAAQS). The current NAAQS for O_3 concentrations ([O_3]) is 75 ppbv, defined as the 3-year average of the annual fourth-highest daily maximum 8 h average (DMA8) [O_3] for each monitoring site within an airshed. The US EPA has already proposed to lower the standard to 65-70 ppbv (EPA 2014) and may also redefine the national O_3 secondary standard for protecting sensitive vegetation and ecosystems (Huang et al., 2013). Currently, many U.S. cities are classified as NAAQS O_3 nonattainment areas based on the 2008 federal standard (http://www.epa.gov/airquality/greenbook/hnc.html). In addition, sensitive areas (e.g., national parks and wilderness areas) also experience DMA8 O_3 exceedances (http://www.nature.nps.gov/air/Monitoring/exceed.cfm). Therefore, improved understanding and attribution of [O_3] sources in these areas is necessary to develop effective air quality management strategies to achieve ever more stringent US air quality standards.

As a secondary pollutant, measured ground-level [O_3] is the result of O_3 production/loss due to local sources of precursor emissions, to transport of O_3 and its precursors from nearby

and/or remote regions, and to ozone formed from natural precursor emissions. The direct way to characterize O_3 source attribution is through field measurements (e.g., Fast et al., 2002; Kemball-Cook et al., 2009; Nunnermacker et al., 2004). The other way to identify transported O_3 and local generated O_3 is to use trajectory models (e.g., MacDonald et al., 2006; Lanford et al., 2010).

Transport of ozone and its precursors from one area to another is determined by flow patterns, which can be obtained by measurement and/or modeling. However, information on flow alone is insufficient in ozone studies because of the complexity of the chemistry involved, wherein ozone and precursors nonlinearly interact with flow, turbulence and sunlight to determine ozone distributions (Huang, et al., 2013; Lee et al., 2003; 2007; Levy II et al., 1985). Chemical transport models (CTMs) are increasingly common in simulating atmospheric chemical and transport processes at regional/continental/global scales because of the detailed physical and chemical processes which they're capable of simulating. For example, using a CTM (GFDL AM3), Lin et al. (2012) found that Asian O_3 pollutants can affect surface [O_3] in the western U.S., contributing up to 8-15 ppbv to the DMA8; and that Asian pollution increases the DMA8 O_3 exceedance days by 53% in the southwestern U.S. Huang et al. (2013), combining model simulations at 12-km resolution (WRF/STEM), remote-sensing, and ground-based observations, have studied the effect of southern California anthropogenic emissions (SoCal) on ozone pollution in southwestern U.S. mountain states. They found that the SoCal precursor emissions and its transported ozone increased [O_3] up to 15 ppbv in western Arizona. They also characterized the nonlinear relationship between emissions and [O_3]. However, these studies

have not examined the impacts of regional emissions on [O_3] in an urban setting (such as Phoenix), at high-resolution.

Physical/chemical-based CTM modeling is the only available tool for ozone transport predictions on finer spatial scales (Lee et al., 2007). Many studies have investigated ozone transport at urban scales using coupled meteorological and chemistry models. For example, Lu et al. (1997) found that ozone and other pollutant concentrations were higher in northern and eastern Los Angeles (LA) than those in the western and central greater LA, where strong emission sources are located, due to transport owing to the persistent onshore sea breeze and mountain-induced upslope flow. Analogously, that surface [O_3] in the Phoenix metropolitan area and its rural environs are higher in northeastern than in southwestern Phoenix arises from transport of urban pollutants by prevailing southwest winds (Fast et al., 2000; Lee et al., 2003 , 2007; Lee and Fernando, 2013). Although these studies have considered both chemistry and transport processes at the urban scale, they did not try to distinguish between ozone produced by local emissions and that produced by regional transport, a principal motivation of this study.

The Phoenix metropolitan area is classified as an O_3 nonattainment area under the 2008 NAAQS primary O_3 standard (http://www.epa.gov/airquality/greenbook/hnc.html). Therefore, it is helpful to separately quantify the relative contributions of local emissions and regional transport to Phoenix [O_3] in order to design feasible and effective ozone control strategies. Both aircraft observations (Nunnermacker et al., 2004) and backward trajectory analysis (MacDonald et al., 2006) indicate that surface [O_3] on exceedance days are attributed to both Arizona local anthropogenic emissions (AZ) and regional and/or continental transport. Therefore, our focus is to use a CTM to separately quantify the contributions of local and regional emissions to the

ozone distributions in Phoenix on exceedance days, research which has not been published in peer-reviewed journals.

In addition, previous studies indicate that coarse-resolution modeling cannot adequately represent the heterogeneities of ozone and meteorological fields in Phoenix due to its complex terrain (Fast et al., 2000; Lee et al., 2003; Lee and Fernando, 2013). That high-resolution CTMs can obtain better results in modeling urban air quality is also reported for the LA basin, Mexico City, and other regions (e.g., Tie et al., 2010; Chen at al., 2013; Lu and Turco, 1995; 1996; Taha, 2008; Klich and Fuelberg, 2014; Stock et al., 2014). Therefore, employing a high-resolution CTM to address air pollutant distributions in the Phoenix metropolitan area due to local emissions and regional transport is our second motivation.

Using WRF-Chem (Grell et al., 2005) at high-resolution, we will examine: (1) the relative contributions of SoCal and AZ to the ozone episodes in Phoenix, and (2) how SoCal (emissions) affect Phoenix [O_3]. This is a topic that has received limited research attention to date (Moore, 2014), but requires investigation because of the metropolitan area's non-attainment ozone status and because of the need to evaluate the effectiveness of local anthropogenic emission control strategies necessary to attain the standard.

2. Methodology

2.1 WRF-Chem setup

We chose WRF-Chem (version 3.5.1) as the CTM since it has been successfully used in this region (Chen et al., 2011; Li et al., 2014; Zhao et al., 2012). In WRF-Chem, the Weather Research and Forecasting (WRF) model (Skamarock et al., 2008) is employed to resolve

atmospheric physics and dynamical processes, while the coupled chemistry (Chem) model is used to simulate chemical processes such as gaseous and aqueous chemical reactions, dispersion, and deposition. The WRF-Chem setup consists of the Lin's cloud scheme (Lin et al., 1983), the RRTM radiation scheme (Mlawer et al., 1997), the Noah land surface model with single layer urban canopy model (Chen and Dudhia, 2001; Chen et al., 2011; Ek et al., 2003), the Grell-Devenyi ensemble cumulus scheme (Grell and Devenyi, 2002) that allows subsidence and spreading at high-resolution, a revised MM5 surface layer, and the BouLac Planetary Boundary Layer (PBL) schemes. Land cover and land use data from the MODIS 1-km resolution dataset (Friendl et al., 2002) are combined with the 2006 National Land Cover Database (NLCD) 3-class urban covers to better represent the urban landscape. The second generation regional acid deposition model (RADM2, Stockwell et al., 1990; Gross and Stockwell, 2003) is used for gas-phase chemical reactions. The aerosol algorithms are based on the MADE/SORGAM (Ackermann et al., 1998; Shell et al., 2001) with GOCART, functioning as an emission scheme that accounts for surface wind speed, soil moisture, and soil erodibility (Ginoux et al., 2001; Zhao et al., 2010). The other selected chemistry schemes are based on the recommendations provided in the WRF-Chem users' guide (Peckam et al., 2013).

Four nested domains are used (Figure 1a). The first (domain 1) has 36-km grid spacing and covers the western and central U.S., eastern Pacific, northern and central Mexico, the Gulf of California, and the western Gulf of Mexico. Nested domains 2, 3, and 4 use grid spacings of 12-km, 4-km, and 1.333-km, respectively. The innermost domain (1.333-km) grid spacing (with 640 by 301 grid cells) encompasses southern California (the South Coast Air Basin or greater Los Angeles Air Basin, the San Diego Air Basin, the southern Mojave Desert Air Basin, the Salton Sea

Air Basin, the southern part of the South Central Air Basin,and the central and southern Arizona airsheds to better represent the complex terrain and land cover features (see Figure 1b). As shown in Figure 1b, the mountainous features in southern California and Arizona are well represented at high resolution. The San Gorgonio Pass (between the San Bernardino Mountains and the San Jacinto Mountains), the Cajon Pass (between the San Gabriel Mountains and the San Bernardino Mountains), and the Newhall Pass (west of the San Gabriel Mountains) are also resolved. The vertical configuration of the model comprised 41 layers: the lowest 15 layers are within 1500 m a.g.l. and the first half-vertical layer above the land surface is at 12.5 m a.g.l. The observation sites (including O_3, NO_x, CO, and surface wind observations) used for validation of the Control simulations are also superimposed (Fig. 1b).

2.2 Data used for model initialization and evaluation

The biogenic emission data are obtained from the 1-km resolution Model of Emissions of Gases and Aerosols from Nature (MEGAN, Guenther et al., 2006). The North American Regional Reanalysis (NARR; Mesinger et al., 2006) product is used for initial and boundary conditions (atmospheric and land surface [e.g., soil moisture and temperature]). NARR data are distributed on a 32-km grid with a 3-hour temporal frequency. The atmospheric chemical boundary and initial conditions are obtained from MOZART-4/GEOS-5 (http://www.acd.ucar.edu/wrf-chem/mozart.shtml) for 2012 case and MOZART-4/NCEPT42 for 2005 case (Emmons et al., 2010).

The anthropogenic emissions used in this study are obtained from 2005 National Emissions Inventories (NEI05) data provided by the U.S. EPA (www.epa.gov/ttnchie1/net/2005inventory.html). These data are distributed on a 4-km grid

array covering the U.S. and surrounding land areas. A method utilized to interpolate the 4-km grid spacing NEI05 data to any resolution one wishes to use for WRF-Chem simulations is provided with the WRF-Chem system (http://www.acd.ucar.edu/wrf-chem/). Each WRF-Chem model grid point data is based on averaging from those NEI05 grid points that fall within a distance less than the WRF-Chem model resolution. The method works well when WRF-Chem grid spacing is coarser than 4-km. However, the method misrepresents emissions when the model resolution is greater than the NEI05 grid. To overcome this issue, we have used Monotonic Cubic Interpolation to downscale the 4-km resolution NEI05 data to a 1.333-km resolution grid (the finest model grid spacing of our WRF-Chem simulations). Details on the NEI05 downscaling method and improved simulation performance are discussed separately (Li et al., 2014).

The data used for model evaluation include measurements of surface wind speed and direction (24 sites within Domain 4). These wind fields are obtained from two networks: the AZMET (ag.arizona.edu/azmet), and the Air Quality and Meteorological Information System (AQMIS) in the California EPA/Air Resources Board (www.arb.ca.gov/aqmis2/aqmis2.php). We use hourly observations of ozone concentrations from 26 stations in Arizona (downloaded from www.epa.gov/ttn/airs/airsaqs/) and 46 stations in Southern California (downloaded from www.arb.ca.gov/aqmis2/aqdselect.php?tab=hourly). In addition, the hourly NO_X observations, including four stations in Arizona and over 20 sites in southern California, and hourly CO observations, including four stations in Arizona and about 20 stations in southern California, can be obtained from the same websites as ozone data. Comparison of simulated and observed VOC concentrations was precluded by the latter's irregular availability and their lack of hourly concentrations.

3. Results and discussion

Two episodes (May 14, 2012, and July 19, 2005) are selected as case studies. The criterion for selection required observed DMA8 [O_3] to exceed 80 ppbv for at least 10 of the reporting stations in the Phoenix metropolitan area. For both events, the synoptic weather in southern California and south-central Arizona was calm, clear, and sunny with light westerly winds within the lower troposphere for the time periods discussed in this section, based on NARR 3-hourly data. In addition, these two events represent the pre-monsoon and monsoon seasons, respectively, two typical climate circulations (Adams and Cowrie, 1997) during the ozone season.

The model (WRF-Chem) is initialized four days prior to each episode with the data of the first 24hours being discarded. In addition, analysis nudging is applied for the meteorological fields (U, V, T, GPH, and Q) above the PBL in the outer-most domain for the first 24 hours.

3.1 Model evaluation

Figure 2 shows the comparison of surface wind fields (circles in Figure 1b) between observations (bold-black) and WRF-Chem simulations (bold-red; i.e., running WRF-Chem with appropriate emissions and hereafter referred to as CTRL) for the selected events. The time periods (labeled in figure 2) cover 4 days, concluding with the episode day in the Phoenix metropolitan area. In comparison with observations, the model appropriately reproduced the diurnal variation with only a slight overestimate of wind speed during daytime. Note that each observation represents a single point while the closest simulation grid cell to the observed latitude/longitude location (representing an area of 1.333 by 1.333-km) is used for comparison.

Although there are some differences between simulated and observed means, the standard deviations for both modeled (thin-red) and observed (thin-black) measurements fall in the same range. Mean Bias (MB), Root Mean Squared Error (RMSE), and correlation coefficient (R) are also calculated and labeled in each panel. For the U-component of wind speed, MB is less than 1.0 m/s and RMSE is about 3.0 m/s (indicating wind heterogeneity within the simulation domain). U-component winds for the CTRL runs and the observations exhibit linear correlations with statistical significance ($P<0.01$). The MB for V-component wind is less than 0.5 m/s. Linear correlation indicates that V-component winds from the model and the observations are statistically significant ($P<0.01$) for the time periods of May 11-14, 2012 and July 16-19, 2005. The wind and temperature comparisons between WRF-Chem in Domain 1 and NARR data are also examined. Generally, the simulations are consistent with NARR data in patterns and magnitudes for the two cases. More specifically, there were continuously westerly winds between the southern California and central Arizona for both NARR and simulations at 850 hPa. Figure S1 is an example of the comparisons of wind and temperature at 850 hPa (bottom panel) and 700 hPa (top panel) for the average of July 16-19, 2005. These comparisons, which indicate sufficiently accurate meteorological simulations, ensure that regional pollutant transport can be adequately simulated, one of our focuses in this study.

Figure 3 shows the comparison of CO, NOx, and O_3 concentrations between the model (bold-red, i.e., CTRL run) and observations (bold-black) in Domain 4 for the same time periods. Note that only four sites of NOx and CO were measured (only one site online available) in greater Phoenix while over 20 sites are found in southern California. On average, the model performed well for both CO and NOx concentrations for the July case. In contrast, for the May case, the

model overestimated CO and NOx during nighttime but matched observations during daytime. The standard deviations (thin-red) from the model are much greater than those from observations (thin-black), indicating that modeled NOx and CO heterogeneity at sites is greater than that from observations. The model behavior in the May case indicates that the anthropogenic emissions could be over-estimated using the NEI05 data due to emission control strategies enacted in California in the seven intervening years (Pusede and Cogen, 2012). Figure S2 shows how the emissions changed between 2005 and 2012 for the South Coast Air Basin, California (http://www.arb.ca.gov/app/emsinv/fcemssumcat2013.php) and 2011 in Maricopa County, Arizona (http://maricopa.gov/aq/divisions/planning_analysis/emissions_inventory/Default.aspx) Relative to 2005, anthropogenic emissions of CO, NOx, and VOC are reduced about 40-50% in 2012 in the South Coast airshed, California. Therefore, the NEI 2005 overestimates [CO] and [NOx]. However, the changes in Maricopa County are not significantly except CO from Mobile.

The [O_3] comparison between observations and simulations presented in Figure 3 indicates the model performed better in simulating [O_3] than CO or NOx. Both the station average and station standard deviation from the model and observations matched each other on event and non-event days (details on site-by-site comparisons in Phoenix will be discussed in the next section). The simulated average [O_3] and their spatial heterogeneities fall within the range of observations except on May 13, 2012, when modeled average [O_3] and the spatial standard deviations fall out of the observation ranges.

Figure S3 shows [O_3] time series separately for southern California and greater Phoenix; corresponding statistics are shown in Table 1. In checking Figure 3, and Figures S2 and S3, although the NEI-2005 over-estimated CO and NOx emissions in 2012 in the south coast airshed,

California, causing [NOx] and [CO] to be over-estimated as well, the ozone simulations nonetheless appear to be quite acceptable. One explanation could be that this airshed is categorized as a VOC-limited ozone environment. Under this condition, ozone concentrations are restrained by VOC concentrations. In other words, reducing NOx fails to reduce ozone concentrations (e.g.,Taha et al., 1998) and the same is also found in Phoenix area (Fast et al., 2000, Lee and Fernando, 2013), which can partly explain why the modeled [O_3] matched the observations, even though the modeled [NOx] and [CO] are highly overestimated in the May case.

Table 1 presents the statistics of comparisons of surface ozone concentrations between the model and observations in southern California (total 46 sites) and greater Phoenix area (total 24 sites), respectively. These statistics are widely used in evaluating model performance (Simon et al., 2012). Our statistics are comparable with those from previous studies in the two regions. For example, in southern California, the mean biases, RSME and correlation coefficients shown in Table 1 are comparable with those from Huang et al.(2013, their Table 3) and Chen et al. (2013, their Tables 2 and 3). Furthermore, the mean normalized bias and mean normalized gross error are comparable with those from Taha (2008, in his Table 2). In greater Phoenix, these statistics are generally comparable with those from Lee et al. (2007), and Li et al. (2014).

To examine the effects of model resolution on surface ozone concentrations, we conducted two additional model runs. These two additional runs were set up and configured exactly the same as the 1.33 km runs; but, with just running WRF-Chem with Domains 1, 2, and 3, which means the highest resolution of model output is 4 km. The model performance at 4 km resolution was also validated against ozone observations and summarized in Table 1. As shown in Table 1, the model performed much better for the

correlation coefficients, normalized mean gross errors, mean normalized bias, and normalized mean error at 1 km than those at 4 km. For the mean bias and normalized mean bias, the model performed better in southern California at 1 km than those at 4km, with similar performance in greater Phoenix. Therefore, we conclude that WRF-Chem in its present configuration performed better at 1 km resolution than that at 4 km resolution, based on the two events and on the 2005 NEI. Our results are consistent with previous studies (e.g., Taha 2008; Tie et al., 2010). In the following analysis and discussion, we mainly focus on the model output at 1km resolution.

The evaluation shown in Figs. 2-3, Figure S3, and the statistical analysis presented in Table 1 demonstrate that the WRF-Chem model, in its current configuration and set up, produces simulated ozone concentrations comparable to the observations.

3.2 Contribution of local and remote emissions to Phoenix [O_3]

Next, we investigate impacts of anthropogenic emissions in southern California (SoCal) and Arizona (AZ) on Phoenix [O_3]. To achieve this goal, we have conducted additional WRF-Chem simulations for the selected cases with the same model setup as presented and evaluated in Sections 2.1 and 3.1, and refer to these experiments as "CTRL", but with (1) exclusion of SoCal emissions (indicated as the dashed-red-line box in Figure 1b) and called "noCA"; (2) exclusion of AZ emissions (indicated as the dashed-black-line box in Figure 1b) and called "noAZ"; and (3) exclusion of all anthropogenic emissions in Domain 4, and called biogenic emissions only (BEO).

Figure 4 shows the hourly [O_3] comparison for observations (Obs), CTRL, noCA, noAZ, and BEO simulations at selected observation sites in the Phoenix area on May 11-14, 2012, (Figure 4a-4f) and July 16-19, 2005 (Figure 4g-4l). Figure 4 indicates that hourly [O_3] from the CTRL run match the observations very well in western downtown (ID0019, ID2001), central downtown

(ID3003, ID9997), and east and north suburban areas (ID9508, ID9702). AZ emissions are the principal contribution to ozone production over Phoenix during daytime (compare the change in simulated [O_3] as demonstrated by the red contour [CTRL] and dashed-blue contour [noAZ]), with a maximum magnitude of up to 40-60 ppbv hourly (compare differences between CTRL and noAZ). The contribution of SoCal emissions to Phoenix [O_3] ranges between 10-40 ppbv during daytime (compare the change in simulated [O_3] as demonstrated by the red contour [CTRL] and green contour [noCA]). Based on the BEO run (gray contour), the contribution of biogenic emissions (including larger-scale lateral input) to Phoenix [O_3] varies between 25-35 ppbv, indicating a baseline target for emission reduction strategies. Following Huang et al (2013), the contribution of SoCal to [O_3] in the Phoenix area is the difference between the CTRL and noCA experiments. The relative contributions from SoCal, AZ, and BEO emissions to hourly [O_3] at observation sites for July 2005 and May 14, 2012 are shown in Figures S4 and S5.

Figure 4, and Figures S4 and S5 indicate the relative contribution of SoCal and AZ emissions to [O_3] vary with time. Physical and chemical processes at each stage can explain this variation. During nighttime, noCA [O_3] are less than that of the noAZ run. This is because there is no ozone consumption (or titration) in the noAZ run while transported ozone can still make its contribution. After sunrise, solar radiation heats the ground surface, increasing the planetary boundary layer (PBL) height. Ozone accumulated within a residual layer from previous day(s) is entrained into the PBL, increasing ground-level [O_3]. This process continues until the PBL height reaches its peak. Simultaneously, ozone production starts with its precursor emissions in the presence of sunlight, a rate that increases with increasing sunlight intensity and surpasses the transport rate of [O_3] by mid to late afternoon. Furthermore, Figure 4 indicates that the peak

time of [O_3] differs between the CTRL run and the noAZ run at some locations for some days. These differences of [O_3] peak time indicate the importance of ozone transport.Figure 5 displays the mean diurnal variation of [O_3] for the different emission scenarios for the two cases. The data are averaged over all urban grid cells (i.e., not solely over the station sites presented in Figure 4) in Phoenix for May 11-14, 2012, and July 16-19, 2005, respectively. The relative contribution of emissions to Phoenix [O_3] are clear and the diurnal features are similar to those shown in Figure 4, Figure S4, and Figure S5, emphasizing the crucial roles of both local and remote emissions.

The daily maximum 8-hr average (DMA8) [O_3] from CTRL and the relative contributions to DMA8 [O_3] from different emission scenarios (BEO, SoCal, and AZ) are assessed at observation sites and for all urban grid cells within Phoenix (Figure 6).The model reproduces observations very well with a slight underestimation on July 19, 2005, but with an overestimation on May 13, 2012. The contribution of SoCal to DMA8 [O_3] in the Phoenix area ranges between 20 – 30 ppbv for the May case and 5 - 20 ppbv for the July case. Relative to the CTRL run, the percentage contributions of 26% - 36% for the May case and 7% - 38% for the July event emphasize the significant effect of southern California emissions on Phoenix metropolitan area air quality. For the two episode days, the contributions are 28 ppb (36%) for May 14, 2012, and 11 ppb (16%) for July 19, 2012. The relative contributions of AZ local emissions to greater Phoenix observation sites are also shown in Figure 6. Overall, the relative contributions of AZ local emissions to Phoenix [O_3] are more than that of SoCal emissions.

The means of DMA8 [O_3] throughout the Phoenix urban area (about 1100 grid cells) arising from the different emission scenarios are shown in Figure 6b and d, and indicate similar values to those at observation sites (Figure 6a, c). The contribution of SoCal emission to DMA8

361 [O_3] for the Phoenix metropolitan area ranges between 20 – 32 ppbv for the May 11-14, 2012,
362 case, and from 6 – 22 ppbv for the July 16-19, 2005, case. The percentages, relative to CTRL, are
363 from 27% to 37% for May 11-14, and from 9% to 40% for July 16-19. Considering only the two
364 days with the maximum ozone concentrations, the contributions are 29 ppb (37%) and 11 ppb
365 (16%) for May 14, and July 19, respectively.

366 Note that in Figure 6, the differences of CTRL minus BEO is not equal the sum of the
367 differences of CTRL minus noCA plus that of CTRL-noAZ. The reason could be the nonlinear
368 processes among emissions, physical, and/or chemical mechanisms (Know et al. 2015) and the
369 uncertainties of the entire system: both the emissions and the models themselves.

370

371 Figure 6 demonstrates the following sults: (1) the impact of AZ emissions on DMA8 [O_3]
372 in the Phoenix area is greater than that of the SoCal's; (2) even so, SoCal emissions considerably
373 increase DMA8 [O_3] in the Phoenix area by up to 30 ppbv, though this is day and case dependent;
374 (3) the DMA8 [O_3] from the BEO experiment are in excess of 30 ppbv, including the contributions
375 of biogenic emissions and lateral boundary transport. Based on the diurnal variations shown in
376 Figures 4 and 5, and Figures S4 and S5, [O_3] due to biogenic emissions could be 10-17 ppbv. In
377 other words, the contribution of BEO emissions to Phoenix DMA8 [O_3] cannot be ignored despite
378 the region's aridity and lack of dense forests. Note that all of these resuts are based on the US
379 EPA 2005 national emissions inventories.

380 Figure 7 depicts the spatial distributions of DMA8 [O_3] for different emission scenarios on
381 July 19, 2005. The CTRL run indicates that higher [O_3] occur in the northeastern urban perimeter,
382 which is consistent with previous studies (e.g. Lee and Fernando 2013). The effects of SoCal

emissions and AZ local emissions on DMA8 [O_3] are location-dependent. The case of May 14, 2012, is also examined (see Figure S6) and a similar distribution as in Figure 7 is found, but it differs in magnitude.

In summary, our results demonstrate that removing SoCal emissions would facilitate attainment of [O_3] in Phoenix on some days, but not on others. In other words, SoCal emissions are an important, if uneven, contributor to the DMA8 [O_3] exceedances for Phoenix. In addition, the effects of SoCal emissions on Phoenix DMA8 [O_3] are location-dependent (see Figure 7 and Figure S6). From a pollution control point of view, our results indicate that reducing the emissions emitted in Phoenix is the key to attain federal standards. With typical synoptic wind fields, emissions from southern California affect ground-level [O_3] in the Phoenix metropolitan area significantly. Therefore, the results indicate that Phoenix would benefit from regional, in addition to local, emission controls to reach NAAQS attainment status.

3.3 Southern California to Arizona [O_3] transport

Through analysis of [O_3] variations with the various emission scenarios, 10-30% of [O_3] in the Phoenix area can be attributed to SoCal emissions for the cases presented here. In this section we will examine pathways characterizing how pollutants in the coastal air basins of southern California are transported into Arizona and affect air quality in the Phoenix area based on 1km resolution model output. The corresponding analyses of the results from the 4 km resolution output can be found in the supplement materials.

Figure 8a shows a Hovmoller diagram of [O_3] differences (CTRL minus noCA) and the wind vector field (from CTRL run) for the May case at the model's 13th vertical level (about 1100 m

above ground-level, or agl) of WRF-Chem along the cross-section B'B (indicated in Figure 1b). The Hovmoller diagram is a suitable technique to identify transport and propagating phenomena in a given field (i.e. Hovmoller, 1949). In Fig.8a, the y-axis is the model integration time (hours) and the x-axis is the location (longitude) along the B'B transect. The approximate locations of Phoenix (PHX), desert, mountains (Mnts) and coast are also labeled in this figure. Since both CTRL and noCA experiments include the same emissions except over California, the difference in ozone between these experiments offsets the chemical ozone production east of California and west of Phoenix. Thus, the residual ozone perturbation field in these regions is dominated by transport. The pattern of this field exhibits tilted ozone bands with phase lines that have consistent positive slopes (Fig. 8a), indicating that a perturbation of ozone in California will eventually reach Arizona. This demonstrates that the residual ozone field shown in Fig. 8a is caused by transport from California to Arizona. The Hovmoller diagram of [O_3] differences for the July case also exhibits patterns of residual ozone with positive slopes indicating transport (Fig. 8b). These slopes are, however, less pronounced than the May case.

The data within each model vertical layer are examined. It is found that peak transport occurs in different model layers depending on the event. For the July event, there is ozone transport from the 5th model layer (about 150 m a. g. l.) to the 13th model layer(1100 m a. g. l.). For the May event, ozone transport occurs from the 5th to 17th (2000 m a. g. l.) model layers. The Hovmoller diagrams for NOx and VOCs indicate that most air masses of NOx and VOCs are horizontally confined near emission source areas and are vertically restricted to below about 1500 m agl (figure not shown), compared to the magnitude presented in Figure 8.

We next examine how pollutants from southern California are transported into south-central Arizona and discuss the physical-chemical mechanisms responsible. Analysis of anthropogenic emission distributions indicates that emissions mainly originate from coastal areas in southern California (also see their Figure 1 in Chen et al. 2013 for emission distribution). Therefore, we first explain how the pollutants cross the coastal mountains and reach the inland desert regions in southern California.

As discussed in Section 1, wind fields are paramount in pollutant transport (Lee et al., 2007). Figure 9 displays the daytime averaged (20Z to 02Z) wind vector field at 40 m a. g. l. in the southern California coastal area of July 16-19, 2005 (for 4 km resolution plots, see Figure S7). The wind patterns exhibit a combination of on-shore ocean breezes and mountain-induced upslope winds, similar to features reported by Lu and Turco (1996) and Lu et al. (1997). The wind field distribution shown in Figure 9 propels pollutants emitted in coastal areas towards the coastal mountains. The polluted air masses can be lofted up to 3-4 km agl over the mountains through the Mountain Chimney Effect (MCE, Lu and Turco, 1996). The pollutants above mountain-top height might either be transported into the free atmosphere over the coast (Lu and Turco, 1996) and/or be transported towards the inland desert and affect the air quality in the desert of southern California (Huang et al. 2013; VanCuren 2014) and of nearby mountain states (Langford et al. 2010; Huang et al. 2013).

The entire transport path, from the southern California coast to south-central Arizona, and the associated ozone vertical distributions along cross-sections A'A, B'B, D'D and E'E, is described here in this subsection. First, vertical distributions of [O_3] along cross-sections A'A and B'B are checked from 21Z to 24Z each day and Figure 10 is an example of vertical distributions of

[O_3] along cross-section A'A and B'B at 22Z on July 17, 2005 (for 4km resolution plots, see Figure S8). Results presented in Figure 10 are similar to those reported by Lu and Turco (1996, in their Figures 4 and 6) from modeling and Langford et al (2010; in their Figure 3) from observations, indicating that WRF-Chem adequately simulates the Mountain Chimney Effect (MCE). Note the distribution of potential temperature contours in Figure 10, illustrating that ozone-laden air masses above mountain peak height may be directly transported into the desert PBL under appropriate flow at these levels. This pattern differs from that of transport back to the free atmosphere over coastal basins (note the tongue of high [O_3] to the west of the peak in Figure 10a). This is because of the particularly high PBL height (in excess of 3-4 km a. g. l.) in the desert during daytime due to strong solar radiation. At nighttime, ozone air masses subsequently subside into the residual layers and/or stable PBL in the desert, and are continuously advected by westerly winds (part of the near-surface ozone will be consumed by titration from NOx and by deposition during nighttime). Importantly, Figure 9 indicates the presence of strong winds from the coast flowing through the mountain passes. For example, there are southerly winds flowing along the Cajon Pass (see location in Figure 1b) and strong westerly winds flowing along the San Gorgonio Pass (see location Figure 1b), which are realistic and consistent with the immense fields of wind turbines there. With the wind pattern shown in Figure 9, ozone in low air layers can be directly transported into the southern Mojave Desert Air Basin (SMDAB, See Figure 1b) from the greater Los Angeles Air Basin (GLAAB) through the Cajon Pass. Ozone can also be transported eastward to the Salton Sea Air Basin (SSAB) from the GLAAB through the San Gorgonio Pass and from the San Diego Air Basin (SDAB) through other passes (see Figure9 for the locations and wind vectors).

To demonstrate the model performance in simulating [O_3] in the passes, Figure 11 presents the hourly comparison of [O_3] between observations and simulations (CTRL) at Crestline, near the Cajon Pass, and Banning Airport, near the San Gorgonio Pass. Figure 11 shows that the simulations and the observations are comparable from July 17 to July 19, 2005. In Figure 11, model simulations with 12-km resolution are also plotted to characterize resolution-dependency. It is clear that with higher-resolution, simulated results are improved above those of coarser resolution, a feature likely due to more accurate ozone transport through the passes.

Figure 12 shows the horizontal distribution of the integrated fluxes of ozone differences ($\int([O_3]_{CTRL}-[O_3]_{noCA})\vec{V_{CTRL}}\,dz$) from the surface to 1400 m agl averaged from (a) 18Z to 02Z and (b) 03Z to 17Z, July 16-20, 2005 (data from the other case May 11-15, 2012 are similar and for 4 km resolution plot, see Figure S9). Figure 12 emphasizes two key aspects of this transport:

(1) There were stronger fluxes in the mountain passes, especially in the San Gorgonio Pass, than any other location, indicating the important contributions of mountain passes to ozone transport. Most recently, VanCuren (2014), based on analysis of ozone observations, also suggests the importance of ozone transported into the MDAB through the passes and has confirmed our model results.

(2) Ozone fluxes are present, originating from the coasts and mountains in southern California, extending southeastward along the SSAB and the SMDAB (Figure 12b), crossing the California-Arizona border near the southern Colorado River, then moving northeastward (Figure 12b) along the Gila river basin, and finally reaching the Phoenix area.

The vertical distribution of pollutants is also evaluated along cross-section D'D in the Salton Sea Valley and cross-section E'E in the Gila River Valley (locations are labeled in Figure 1b). Presenting vertical distributions of VOC, NOx and O_3 along D'D on July 18 from CTRL, Figure 13 depicts the transport of the pollutants from late afternoon to midnight, as indicated by the location of high concentration fronts(for the Ccrresponding 4 km resolution plots, see Figure S10) The NOx masses are vertically confined to below 1-km above sea level (asl) with concentrations of 5-15 ppbv. VOC plumes are confined below 2-km asl with concentrations of 10-20 ppbv. We also evaluated the vertical distribution of VOC from the BEO emissions experiment: the vertical distribution is similar to the VOC shown in Figure 13, but the concentrations are about 10 ppbv (figure not shown). In other words, there are about 10 ppbv of VOC that are transported from coastal anthropogenic emissions to this region. Similar to NOx concentrations, the highest concentrations of VOC are near the ground surface.

Ozone vertical distributions reach up to 2-3 km asl with concentrations as high as 90 ppbv. The high [O_3] is centered 1-2 km asl during nighttime while [O_3] is low near ground-level due to the chemical titration by NOx and dry deposition (Figure 13). In other words, among the three pollutants, ozone is most "long-lived" and NOx has the shortest span, which is consistent with their atmospheric chemistry and previous results (e. g., Lee and Fernando, 2013).

The diurnal variation of a pollutant is, in part, a consequence of diurnal variation of flow (the other principal influence is the diurnal variation of the emissions themselves). During daytime, southeasterly winds (valley winds) at lower layers in the northern Salton Sea basin hinder the pollutants from being transported southeastward along the Salton Sea Basin (See Figure 12a and Figure 9). Therefore, a portion of the pollutants, transported from the GLAAB

through the San Gorgonio Pass, accumulate over the northern Salton Sea basin (as shown at 01Z in Figure 13), while a different portion of the pollutants crossed the Little San Bernardino Mountains and reached the SMDAB due to upslope flow (see Figure 12a and Figure 9). During nighttime, basin-scale mountain downslope winds transport the pollutants southeastward along the SSAB basin (Figure 12b and Figure 13).

Figure 14 is similar to Figure 13 but presents results for the cross-section E'E in the Gila River basin in Arizona (location shown in Figure 1b) on July 18 (corresponding 4 km resolution plots, see Figure S11). During this time period, although concentrations of pollutants continued to decrease along this transport pathway, the ozone transport phenomenon was still very clear along the Gila River basin due to the prevailing nighttime southwesterly winds (see Figure 12). These southwesterly winds can result from either the low-level jet from the northern Gulf of California during monsoon season (mid-July to mid September), Adams and Comrie, 1997) or by the inertia from a remnant of daytime westerly winds during pre-monsoon season (from May to mid July , Lee and Fernando, 2013). At about 18Z, the ozone in the residual layer mixes with PBL ozone generated by local photochemical reactions, and finally affects the ground-level concentrations in Phoenix and its surrounding rural areas.

The results presented in this section are mainly based on model simulations. In past decades, there were a few field experiments conducted to measure the vertical distributions of meteorological fields and trace gasses in southern California (e.g., the southern California Air Quality Study in 1987 [Lawson, 1990]; the southern California Ozone Study in 1997[Groes and Fujita, 2003] and CALNEX-2010[www.esrl.noaa.gov/csd/calnex/]) as well as in the Phoenix area (e.g., Phoenix Air Flow Experiment II in 1998 [Fast et al. 2000; Nunnermacker et al., 2004]). Some

of the events during the experiments have been used to address ozone transport (e.g., Huang et al. 2013; Langford et al., 2010) from the southern California coast. No aloft measurements could be found for May 2010 that would be of help in the present model performance evaluation. In addition, satellite-retrieved data may be used to demonstrate the vertical distributions and even distant transport (e.g., Huang et al., 2013), although these data are hampered by limitations such as coarse-resolution, accuracy, etc. (e.g., Bowman, 2013). To quantitatively examine the transport and vertical distribution from southern California coasts to Phoenix, field observations, especially measurements aloft, along the inland California desert region and within western Arizona are needed.

4. Conclusion

As with other cities, Phoenix's ozone concentrations on exceedance days can be attributed to both local precursor emissions and to the transport of ozone and its precursors from remote regions. In this study, WRF-Chem at high-resolution (~1.333-km grid spacing) is employed to investigate surface ozone distributions in southern California and south-central Arizona for two selected Phoenix episodes. Model simulations have been compared with surface observations of hourly ozone, CO, NO_X and wind fields in southern California and Arizona. The results indicate that the WRF-Chem configuration in this study can adequately simulate the spatial distribution, the magnitude, and the variability of the observations. The modeled ozone concentrations ([O_3]) are comparable with previous studies in the focus region.

Three sensitivity studies have been conducted to separate the contributions of southern California anthropogenic emissions (SoCal), of the Arizona local anthropogenic emissions (AZ),

and of biogenic emissions to Phoenix [O_3] on the exceedance days: (1) running WRF-Chem as CTRL but excluding SoCal emissions (noCA), (2) running WRF-Chem as the Control simulation but excluding AZ emissions (noAZ) and (3) running WRF-Chem as the Control simulation but excluding all anthropogenic emissions in domain 4 areas, leaving the biogenic emissions only (BEO). Our simulations indicate that AZ emissions play the key role in formation of the elevated [O_3] in Phoenix for the selected cases (see Figures 4, 5, and 6). Based on the US EPA 2005 emissions inventories, SoCal emissions contribute to DMA8 [O_3] in the Phoenix area, and this impact varies between 5-30 ppbv at various observation sites and from 6-32 ppbv throughout the urban setting. In addition, our model simulations indicate the effects of SoCal emissions on DMA8 [O_3] in Phoenix are location and event dependent, but not negligible. The effects of BEO contributions to Phoenix DMA8 [O_3] are also significant in spite of the region's aridity. The model results are based on the 2005 U.S. National Emissions Inventories (NEI 2005). With more stringent emission control strategies in California, the effects of the pollutants transported from California could be reduced.

The time series of [O_3] of the relative contributions to Phoenix [O_3] from SoCal and AZ emissions exhibit a diurnal variation. During nighttime hours, the transported ozone increases [O_3] while local NOx emissions consume it. The reverse occurs during afternoon hours when locally generated emissions predominate.

WRF-chem's high resolution resolves all pertinent topographical features, especially the critical low-elevation mountain passes, capturing the pollutant transport through them. Therefore, the pollutant's (mainly ozone) transport pathway in the lower troposphere is identified: The pollutants (mainly ozone) are first transported to the southern Mojave Desert Air

Basin (SMDAB) and the Salton Sea Air Basin (SSAB) through both the Mountain Chimney Effect (MCE) and Mountain Pass Channel Effect (PCE) during daytime, affecting DMA8 [O_3] in these two air basins. The following physical transport paths (based on the two events) are: the pollutants are first transported southeastward along the two air basins (the SSAB and the SMDAB) in CA during nighttime, then northeastward along the Gila River basin in AZ during nighttime, and finally reach the Phoenix area and mix with the local air mass by turbulent mixing during daytime. The entire transport path is determined by a combination of local and synoptic circulations.

Since the PBL height can extend in excess of 3-4 km agl in desert air basins, pollutants may be directly transported into the daytime desert PBL from coasts by both PCE and MCE. Therefore, regional transport in the desert is accomplished in the PBL (daytime), and residual layer and stable PBL (nighttime).

This study indicates that in evaluating local emission controls in Phoenix, one should consider emission controls outside Phoenix (i.e., regional controls) and account for the effects of biogenic emissions in addition to local release of pollutants. Not to do so would lead to false expectations of attaining the NAAQS ozone standard, especially when new standards are more stringent.

Acknowledgements: This work has been funded by National Science Foundation grants DMS-1419693, BTS-0215, EAR-1204774 and EF-1049251. We thank the Julie Ann Wrigley Global Institute of Sustainability at Arizona State University for valuable support. The authors appreciate the comments and suggestions from Dr. Steven Peckham (NOAA). Dr. Chun Zhao (PNNL) and Dr. Xiaohong Liu (University of Wyoming) have also shared their successful experiences with the first author. The authors appreciate Dr. Kirk Baker in EPA and the anonymous reviewer for their comments, suggestions and discussions in formalizing the final version

References

Ackermann, I., Hass, H., Memmesheimer, M., Ebel, A., Binkowski, F., and Shankar, U.: Modal aerosol dynamics model for Europe: Development and first applications, Atoms. Environ., 32, 2981-2999,1998.

Adams, D., and Cowrie, A.: The North American monsoon, BAMS, 78(10), 2198-2213,1997.

Anderson, H.: Air pollution and mortality: A history, Atmos. Environ., 43,143-152, doi:10.1016/j.atmosenv.2008.09.026,2009.

Ashmore, M. : Assessing the future global impacts of ozone on vegetation, Plant Cell Environ., 29, 949-964, doi:10.1111/j.1365-3040.2005.01341.x.,2005.

Avnery, S., Mauzeral, D., Liu, J., and Horwiz, W. : Global crop yield reductions due to surface ozone exposure: 1: Year of 2000 crop production losses and economic damage, Atmos. Eviron., 45, 2284-2296,2011.

Bowman, K.: Toward the next generation of air quality monitoring: Ozone, Atmos. Environ., 80, 571-583, 2013.

Chameides, W., Li, X., Tang, X., Zhou, X, Luo, C., Kiang, C., St John, J., Saylor, R., Liu, S., Lam, K, Wang, T., and Giorgi, F. : Is ozone pollution affecting crop yields in China? *G*epphys. Res. Lett., 26, 867-870, doi:10.1029/1999gl900068,1999.

Chen D. , Li Q., Stutz J. , Mao Y., Zhang L., Pikelnaya O., and Tsai J.: WRF-Chem simulation of NOx and O3 in the LA basin during CalNex 2010, Atmos. Environ., 81**,** 421-432.,2013.

Chen F., and Dudhia J.: Coupling an Advanced Land Surface Hydrology Model with the Penn State NCAR MM5 Modeling System. Part 1: Model Implementation and Sensitivity, Mon. Weather Rev*.,* 129**,** 569–585,2001.

Chen F., Kusaka H., Bornstein R., Ching J., Grimmond C., Grossman-Clarke S., Loridan T., Manning K., Martilli A., Miao S., Sailor D., Salamanca F., Taha H., Tewari M., Wang X., Wyszogrodzki A., and Zhang C.: The integrated WRF/urban modeling system: development, evaluation, and applications to urban environmental problems, International J. Climatol., 31(2), DOI: 10.1002/joc.2158., 2011.

Cores B., and Fujita E.: Overview of the 1997 southern California ozone study(SCOS97-NARSTO), Atmos. Environ.,37,3-26.doi:10.1016/S1352-2310(03)00379-0., 2003.

Ek M., Mitchell B., Lin K., Rogers Y., Grunmann E., Koren P., Gayno V. , and Tarpley J.: Implementation of Noah land surface model advances in the National Centers for Environmental Prediction operational mesoscale Eta Model, J. Geophys. Res., 108**,** 8851, doi:10.1029/2002JD003296, 2003.

Emmons L., Walters S., Hess P., Lamarque J., Pfister G., FillmoreD., Granier C., Guenther A., Kinnison D., Laepple T., Orlando J., Tie X., Tyndall G., Wiedinmyer C., Baughcum S. L., and Kloster S.: 2010: Description and evaluation of the model for ozone and related chemical traces, version 4 (MOZART-4), Geosci. Model Dev., 3**,** 43-67,2010.

EPA, 2014: National Ambient Air Quality Standards for Ozone, available online (http://www.epa.gov/glo/pdfs/20141125proposal.pdf)

Fast J., Doran J., and Shaw W.: The evolution of the boundary layer and its effect on air chemistry in the Phoenix area, J. Geophys. Res., 105(D18), 22833-22848,2000.

Fast J., Zaveri D., Bian X., Chapman E., and Easter R, 2002: Effect of regional-scale transport on oxidants in the vicinity of Philadelphia during the 1999 NE-OPS field campaign, J. Geophys. Res., 107(D16) 4307, doi:10.1029/2001JD000980, 2002.

Friedl M., McIver D., Hodges F., Zhang X., Muchnoey D. , Strahler A., Woodcock C., Gopal S., Schneider A., Cooper A., Baccini A., Gao F., and Schaaf C.: Global land cover mapping from MODIS: algorithms and early results, Remote Sens. Environ., 83, 287–302,2002.

Ginoux P., Chin M., Tegen I., Prospero J., Holben B., Dubovik O., and Lin S-J.: Sources and global distributions of dust aerosols simulated with the GOCART model, J. Geophys. Res., 106**,** 20255–20273,2001.

Grell G., and Devenyi D.: A generalized approach to parameterizing convection combining ensemble and data assimilation techniques, Geophys. Res. Lett., 29**,** 4pp. doi:10.1029/2002GL015311, 2002.

Grell G., Peckham S., Schmitz R. , McKeen S., Frost G. , Skamarock W., and Eder B.: Fully coupled "online" chemistry within the WRF model *Atmos. Environ.* **39,** 6957–6975, doi:10.1016/j.atmosenv.2005.04.027, 2005.

Gross A., and Stockwell W.: Comparison of the EMEP, RADM2 and RACM mechanisms, *J. Atmos. Chem.,* 44(2), 151-170, 2003.

Guenther A., Karl T. , Harley P. , Wiedinmyer C. , Palmer P., and Geron C., 2006: Estimates of global terrestrial isoprene emissions using MEGAN (Model of Emissions of Gases and Aerosols from Nature), Atmos. Chem. Phys., 6**,** 3181–3210, doi:10.5194/acp-6-3181-2006, 2006.

He, H., Sehr, L., Hains, J., Krask, D., Dodridge, B., Vinnikov, K., Canty, T., Hosley, K., Salawitch, R., Worden,H., and Dickerson, R.: Trends in emissions and concentrations of air pollutants in the lower tropospheric in the Baltimore/Washington airshed from 1997-2011, Atoms. Chem. Phys., 13, 7859-7874, 2013.Huang, M., Bowman, K., Carmichael, G.,

Pierce, B., Worden, H., Lou, M., Cooper, O., Pollack, I. Ryerson, T., and Brown, S.: Impact of Southern California anthropogenic emissions on ozone pollution in the mountain states: Model analysis and observational evidence from space, J. Geophys. Res-Atmos., 118, 12784-12803, 2013.

Hovmoller, E, 1949: The trough-and-Ridge diagram, Tullus, 1(2), 62-66.

IPCC: Climate change, 2007: The physical science basis, contribution of Working Group I to the Fourth Assessment Report (AR4) of the Intergovemental Pannel on Cimate Change, 996pp.

Kemball-Cook S., Parrish D., Ryerson T., Nopmongool U., Johnson J., Tai E., and Yarwood G.: Contributions of regional transport and local sources to ozone exceedances in Houston and Dallas: Comparison of results from a photochemical grid model to aircraft and surface measurement, J. Geophys. Res*.,* 114**,** D00F02 doi:10.1029/2008JD010248, 2009.

Klich C., and Fuelberg H.: The role of horizontal model resolution in assessing the transport of CO in a middle latitude cycle using WRF-Chem, Atmos. Chem. Phys*.,* 14, 609-627, 2014.

Kwok R., Baker K., Napelenok S., and Tnonnesen G.: Photochemical grid model implementation and application of VOC, NO x, and O 3 source apportionment, Geosci. Model Dev*,* 8: 99-114. doi:10.5194/gmd-8-99-2015, 2015.

Langford A., Senff C., Alvarez R., Banta R., and Hardesty R.: Long-range transport of ozone from the Los Angeles Bsin: A case study, *Geophys. Res. Lett*, 37, L06807,doi:10.1029/2010GL042507, 2010.

Lawson D., 1990: The southern California air quality study, J. Air Waste Manage. Assoc., 40,156-165, 1990.

Lee S., Fernando H., Princevac M., Zajic D., Sinesf M., Mcculley J. and Anderson J. : Transport and diffusion of ozone in the nocturnal and morning planetary boundary layer of the Phoenix Valley, Environ. Fluid Mech., 3 331-362, 2003.

Lee S., and Fernando H.: Dispersion of an urban photochemical plume in Phoenix metropolitan area, Atmos. Environ., 80**,** 152-160, 2013.

Lee S., Fernando H., and Grossman-Clarke S.: MM5-SMOKE-CMAQ as a modeling tool for 8-h ozone regulatory enforcement: application to the state of Arizona, Environ. Model. Assess*.,* 12**,** 63-74, 2007.

Levy II H., Mahlman J., Moxim W., and Liu S.: Tropospheric Ozone: The role of transport. J. Geophys. Res., 90(D2), 3753-3772.,1985.

Li J., Georgescu, M., Hyde P., Mahalov A., and Moustaoui M.: Achieving accurate simulations of urban impacts on ozone at high resolution. *Environ. Res. Lett*. 9(2014),114019, 2014.

Lin Y., Farley R., and Orville H. : Bulk parameterization of the snow field in a cloud model *J. Climate Appl. Meteor.* 22, 1065–1092, 1983.

Lin, M., Fiore, A., Horowitz, L., Cooper, O., Naik, V.,Holloway, J., Johnson, B., Middlebrook, A., Oltmans, S., Pollack, I., Ryerson, T., Warner, J., Wiedinmyer, C., Wilson, J., and Wyman, B.: Transport of Asian ozone pollution into surface air over the western United States in Spring, J. Geophys. Res., 117, D00V07, doi:10.29/2011JD016961, 2012.

Lu R., and Turco, R.: Air pollution transport in a coastal environment: Part II: Three-dimensional simulations of sea-breeze and mountain effect. Atmos. Environ., 29B, 1499-1518, 1995.

Lu R., and Turco R.: Ozone distributions over the Los Angeles Basin: Three-dimensional simulations with the SMOG model, Atmos. Environ., 30(24), 4155-4176, 1996.

Lu R., Turco R., and Jacobson M.: An integrated air pollution modeling system for urban and regional scales: 2: Simulations for SCAQS 1987, J. Geophys. Res., 102(D5), 6081-6098, 1997.

MacDonald C., Miller, D., and Raffuse, D.: Regional and local contributions to peak local ozone concentrations in six western cities. *Final Report for Western States Air Resources Council (WESATR), STI-906004-2970-FR*, Sonoma Technology, Inc. (www.sonomatech.com), 2006.

Mauzerall D., and Wang, X.: Protecting agricultural crops from the effects of tropospheric ozone exposure: Reconciling science and standard setting in the United States, Europe, and Asia, Ann. Rev. Energy Environ., 26, 237-268, 2001.

Mesinger F., DiMego, G., Kalney, E., Mitchell, K., Shafran, P., Ebisuzaki, W., Jovic, D., Woollen J., Rogers, E., Berbery, E., Ek, M., Fan, Y., Grumbine, R., Higgins, W., Li, H., Lin, Y., Manikin, G., Parrish, D., and Shi, W.: North American regional reanalysis, *Bull. Amer. Meteor. Soc.,* 87**,** 343-360, 2006.

Mlawer E., Taubman S., Brown P., Iacono M., and Clough S.: Radiative transfer for inhomogeneous atmospheres: RRTM, a validated correlated–k model for the longwave, J. Geophy. Res.– Atmos., 102**,** 16663–16682, 1997.

Moore, T.: Ozone 301, Maricopa County Air Quality Department, September 4, 2014 (available: http://www.wrapair2.org/WestJumpAQMS), 2014.

Nunnermacker L., Weinstein-Lloyd J., Kleinman L., Daum P., Lee Y., Springston S., Klotz P., Newman L., Neuroth G., and Hyde P.: Ground-based and aircraft measurements of trace gases in Phoenix, Arizona (1998), Atmos. Environ., 38, 4941-4956, 2004.Peckam, S., Grell, G., McKeen, S., Ahmadov, R., Barth, M., Pfuster, G., Wiedinmyer, C., Fast J Gustat]fason, W., Ghan, S., Zaveri, R., Easter, R., Barnard, J., Chapman, E., Hewson, M., Schmitz, R., Salzmann, M., Beck, V., Freitas, S., Previsao de, C., and Estudos, T.:WRF/CHEM Version 3.5 User's Guide, available at: ruc.noaa.gov/wrf/WG11/Users guide.pdf (last access: 12 February 2013), 2013.

Pusede A., and Cogen R.: On the observed response of ozone to NOx and VOCs reductions in San Jaquan Valley California 1995-present, Atmos Chem. Phys., 12, 8323-8339, 2012.

Schell B., Ackermann I., Hass H., Binkowski F., and Ebel, A.: Modeling the formation of scecondary organic aerosol with a comprehensive air quality modeling system, *J. Geophys. Res*., 106, 28275-28293, 2001.

Skamarock W., Klemp J., Dudhia J., Gill D., Barker D., Wang W. and Powers J.: A description the Advanced Research WRF version 3, www.mmm.ucar.edu/wrf/users/docs/arw_v3.pdf, 2008.

Smith, K., Jerrett, M., Anderson, R., Burnett, R., Stone, V., Derwent, R., Atkinson, R., Cohen, A., Shonko, S., Krewski, D., Pope, III, A., Thun, M., and Thurston, G.: Public benefits of strategies to reduce greenhouse-gas emissions: Health implications of short-lived greenhouse pollutants, *Lancet*, 374(9707), doi:10.1016/S0140-6737(09)61716-5, 2009.

Stock Z., Russo M., and Pyle J.: Representing ozone extremes in European megacities: the importance of resolution in a global chemistry climate model, Atmos. Chem. Phys., 14, 3899-3912, 2014.

Stockwell W, Middleton P. , Chang J., and Tang X.: The Second Generation Regional Acid Deposition Model Chemical Mechanism for Regional Air Quality Modeling, J. Geophys. Res., 95, 16343–16367, 1990.

Taha H.: Urban surface modification as a potential ozone air-quality improvement strategy in California: A mesoscale modeling study, Boundary-layer Meteorol., 127, 219-239, 2008.

Taha H., Konopacki S, and Akbari H.: Impacts of lowered urban air temperature on precursor emission and ozone air quality. J. Air Waste Manage. Assoc., 48, 860-865, 1998.

Tie, X., G. Brasseur, G., and Ying, Z., 2010: Impact of model resolution on chemical ozone formation in Mexico City: application of the WRF-Chem model, Atmos. Chem. Phys., 10, 8983-8995, 2010.

Zhao C., Liu X., and Leung R. 2012: Impact of the desert dust on the summer monsoon system over the southwestern North America, Atmos. Chem. Phys., 12, 3717-3731, 2012.

Zhao C., Liu, X., Leung R, Johnson B., McFarlane S., Gustafson Jr W., Fast J., and Easter R., 2010: The spatial distribution of mineral dust and its shortwave radiative forcing over North Africa: modeling sensitivities to dust emissions and aerosol size treatments, Atmos. Chem. Phys., 10, 8821-8838, 2010.

Table 1: Statistical results of hourly ozone concentrations of WRF-Chem simulations (CTRL) at 1km and 4km resolution.

	11-14, May 2012				16-19, July 2015			
	CA	CA	AZ	AZ	CA	CA	AZ	AZ
	1km	4km	1km	4km	1km	4km	1km	4km
Mean Bias (ppb)	-1.9	-3.4	0.6	-0.4	-2.0	-4.0	-4.8	-4.7
Normalized Mean Bias (NMB)	-7.9	-13.5	2.5	-1.7	-8.6	-16.3	-18.5	-18.4
Normalized Mean Error (%)	16.3	25.0	15.4	16.8	24.2	34.1	24.1	25.6
Mean Normalized Bias (%)	-6.7	-10.7	3.2	-1.2	-3.5	-9.7	-16.4	-18.5
Mean Normalized Gross Error (%)	16.7	24.9	15.9	17.3	23.8	34.0	24.5	26.2
Correlation coefficient	0.75	0.54	0.76	0.65	0.74	0.4	0.75	0.61
Root Mean Square Error (ppb)	16.1	19.9	15.7	15.5	22.9	30.1	15.8	17.2

Captions

Figure 1a: 4-nested model domains--D01 to D04, from the largest rectangle box to the smallest rectangle box.

Figure 1b: Innermost domain terrain elevation (m). Black dots indicate the locations of CO, NOx, and/or O_3 observation sites. Circles represent surface wind observation sites. Red-dashed-line box shows the southern California and black-dashed-line box stands for southern and central Arizona. SGM stands for the San Gabriel Mountains; SBM indicates the San Bernardino Mountains; LSBM indicates the Little San Bernardino Mountains; SJM represents the San Jacinto Mountains. SGP stands for the San Gorgonio Pass, between SBM to the north and SJM to the south. CP represents the Cajon Pass between SGM to the west and SBM to the east. PHX stands for Phoenix metropolitan area. Lines A'A, B'B, D'D, and E'E are cross-section locations and are discussed in text and Figures 7, 9, 12 and 13, respectively.

Figure 2: Surface wind comparisons between simulations (bold-red) and observations (bold black). There are totally 20 sites, including those in CA and AZ with locations shown in Figure 1b as circles. The variation ranges of simulation and observation are correspondently labeled by thin-red-line and thin-black-line, respectively. Mean Biases (MB), RMSE and correlation coefficient (R) are labeled also. CTRL represents WRF-Chem control run.

Figure 3: The comparisons of CO, NOx, and O_3 concentrations between observations (bold black) and simulations (bold red) in Domain 4. There are 23 sites for NOx, 20 sites for CO, and

65 sites for O_3 observations during the study time periods. The locations are shown in Figure 1b. The variation ranges of simulation and observation are correspondently labeled by thin-red-line and thin-black-line, respectively. Missing observation time (4:00 local time) is masked in the figure. CTRL represents WRF-Chem control run.

Figure 4: Relative contributions of different emission scenarios to [O_3] at observation sites in Phoenix metropolitan area and surrounding rural areas. The dates are May 11-14, 2012 (Figure 4a-4f) and July 16-19, 2005(Figures 4g-4l). Idxxxx corresponds to the EPA AIRS site number in Maricopa County, Arizona. Black line indicates the [O_3] observation. Red line represents the simulated [O_3] for the CTRL run. Blue line shows the [O_3] for the noAZ run. Green line displays the [O_3] for the noCA run. Gray line is the [O_3] for the BEO run.

Figure 5: Simulated diurnal variations of [O_3] at Phoenix urban setting for different emission scenarios: (a) average from July 16-19, 2005, and (b) average from May 11-14, 2012.

Figure 6: Mean DMA8 [O_3] in Phoenix metropolitan area from observation (Obs), simulation from CTRL runs (CTRL), BEO runs (BEO), and the relative contributions of different emission sources. CTRL-noAZ represents the modeled DMA8 [O_3] differences between CTRL run and noAZ run. CTRL-noCA displays the modeled DMA8 [O_3] differences between CTRL run and noCA run. Observation sites show in Figure 1b. (a) DMA8 {O3] at observation sites for July 16-19, 2005, (b) the same as (a) but for that averaged from Phoenix urban grid cells. (c) and (d), the same as (a) and (b) but for the case of May 11-14, 2012.

Figure 7: DMA8 [O3] spatial distributions in Greater Phoenix and surround areas on July 19, 2005: (a) CTRL, (b), noAZ, (c) noCA, (d) BEO, (e) CTRL-noAZ, and (f) CTRL-noCA. Contours represent terrain elevations. Dots shows O3 observation site. Circle indicates the approximate location of Phoenix urban area.

Figure 8: Hovmoller diagram of [O_3] differences (CTRL minus noCA) at 13th vertical model layer (about 1100-m agl) along the cross-section B'B shown in Figure 1b for July case (top) and May case (bottom). Approximate locations of Phoenix (PHX), desert, mountains (Mnts), and coast are also labeled in Figure 7. The integrating is counted from 00Z, May 10, 2012, and 00Z, July 15, 2005, respectively.

Figure 9: Wind vector field at 40-m above surface layer in southern California coastal area. Data are averaged from 20Z to 02Z, July 16-20, 2005.

Figure 10: Vertical distributions of ozone along cross-section A'A (Figure 9a) and B'B (Figure 9b) shown in Figure 1b at 22Z of July, 17, 2005. The contours are potential temperature starting at 280-K with 1-K interval.

Figure 11: Ground-level ozone concentration comparisons between observations and simulations at (a) Banning Airport (ID0650012, 33.92077^o, -116.85841^o) located in the San

Gorgonio Pass and (b) Crestline (ID060710005, 34.24313°,-117.2723°) near Cajon Pass from July 17-19, 2005. Obs indicates the observation. CTRL represents the simulations from CTRL run and M12km is the model simulations at 12-km resolution.

Figure 12: Integrated fluxes of ozone differences (CTRL-noCA) from surface to 1400 m above ground-level: (a) average from 18Z to 02Z, July 16 to July 20, 2005, and (b) average from 03Z to 17Z, July 16 to July 20, 2005.

Figure 13: The vertical distribution of VOC (top), NOx (middle), and O_3 (bottom) along the cross-section D'D (shown in Figure 1b) in Salton Sea Basin at 01Z, 03Z, and 06Z, July 18, 2005. Contours are potential temperature with 1-K interval.

Figure 14: The vertical distribution of VOC (top), NOx (middle), and O_3 (bottom) along the cross-section D'D (shown in Figure 1b) in Gila River Basin, Arizona at 05Z, 11Z, and 18Z, July 18, 2005. Contours are potential temperature with 1-K interval.

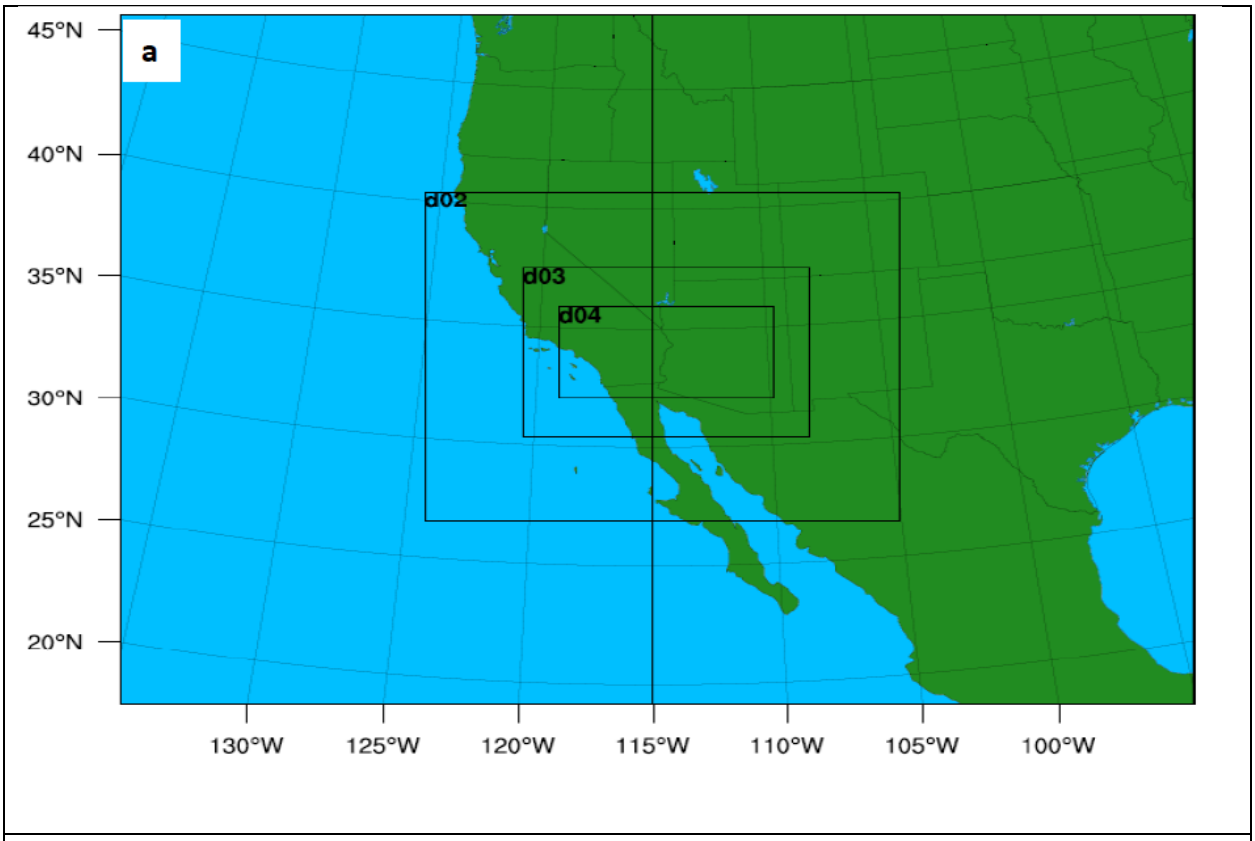

Figure 1a: 4-nested model domains--D01 to D04, from the largest rectangle box to the smallest rectangle box.

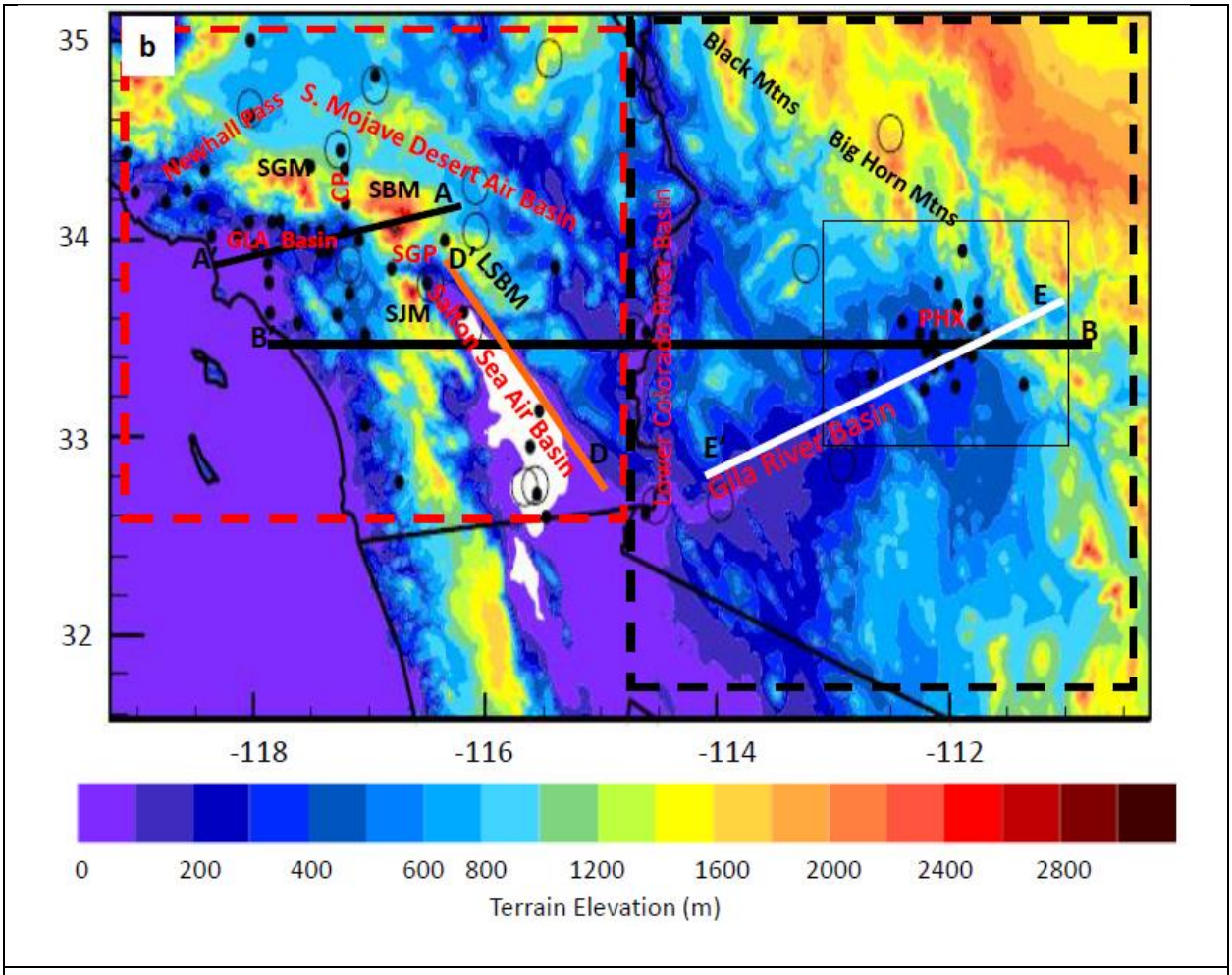

Figure 1b: Innermost domain terrain elevation (m). Black dots indicate the locations of CO, NOx, and/or O_3 observation sites. Circles represent surface wind observation sites. Red-dashed-line box shows the southern California and black-dashed-line box stands for southern and central Arizona. SGM stands for the San Gabriel Mountains; SBM indicates the San Bernardino Mountains; LSBM indicates the Little San Bernardino Mountains; SJM represents the San Jacinto Mountains. SGP stands for the San Gorgonio Pass, between SBM to the north and SJM to the south. CP represents the Cajon Pass between SGM to the west and SBM to the east. PHX stands for Phoenix metropolitan area. Lines A'A, B'B, D'D, and E'E are cross-section locations and are discussed in text and Figures 7, 9, 12 and 13, respectively.

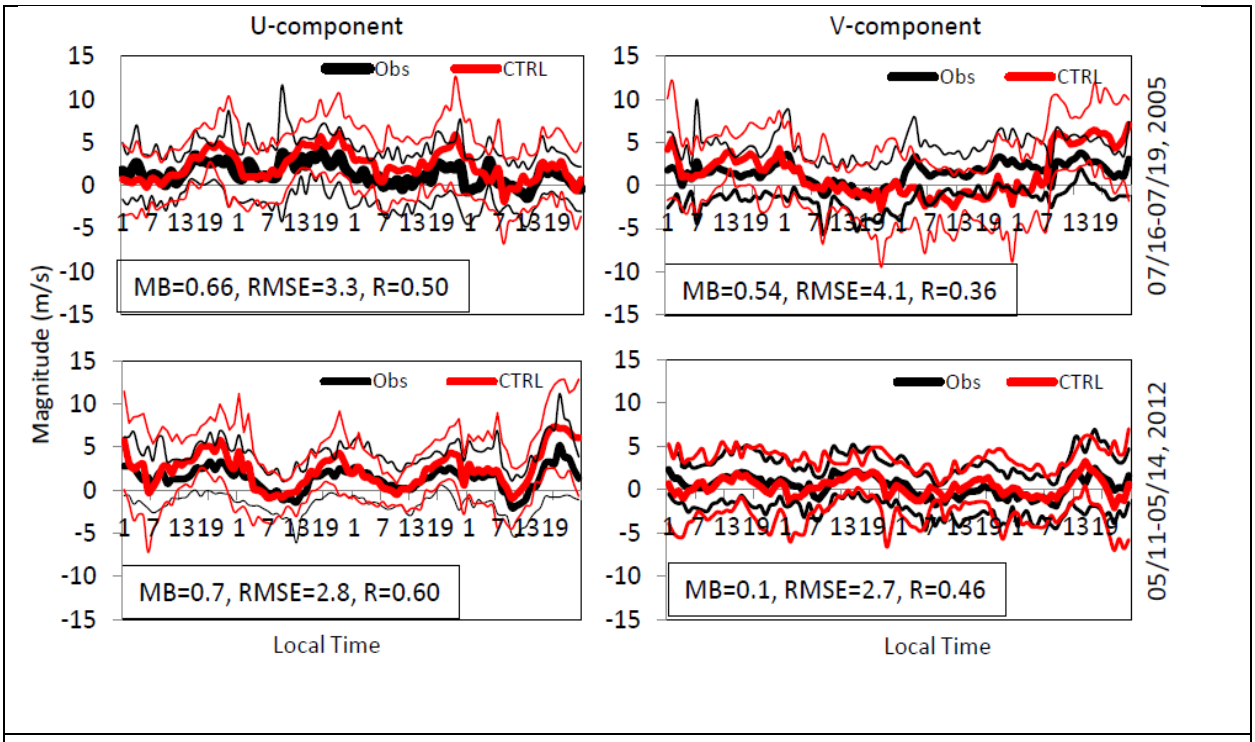

Figure 2: Surface wind comparisons between simulations (bold-red) and observations (bold black). There are totally 20 sites, including those in CA and AZ with locations shown in Figure 1b as circles. The variation ranges of simulation and observation are correspondently labeled by thin-red-line and thin-black-line, respectively. Mean Biases (MB), RMSE and correlation coefficient (R) are labeled also. CTRL represents WRF-Chem control run.

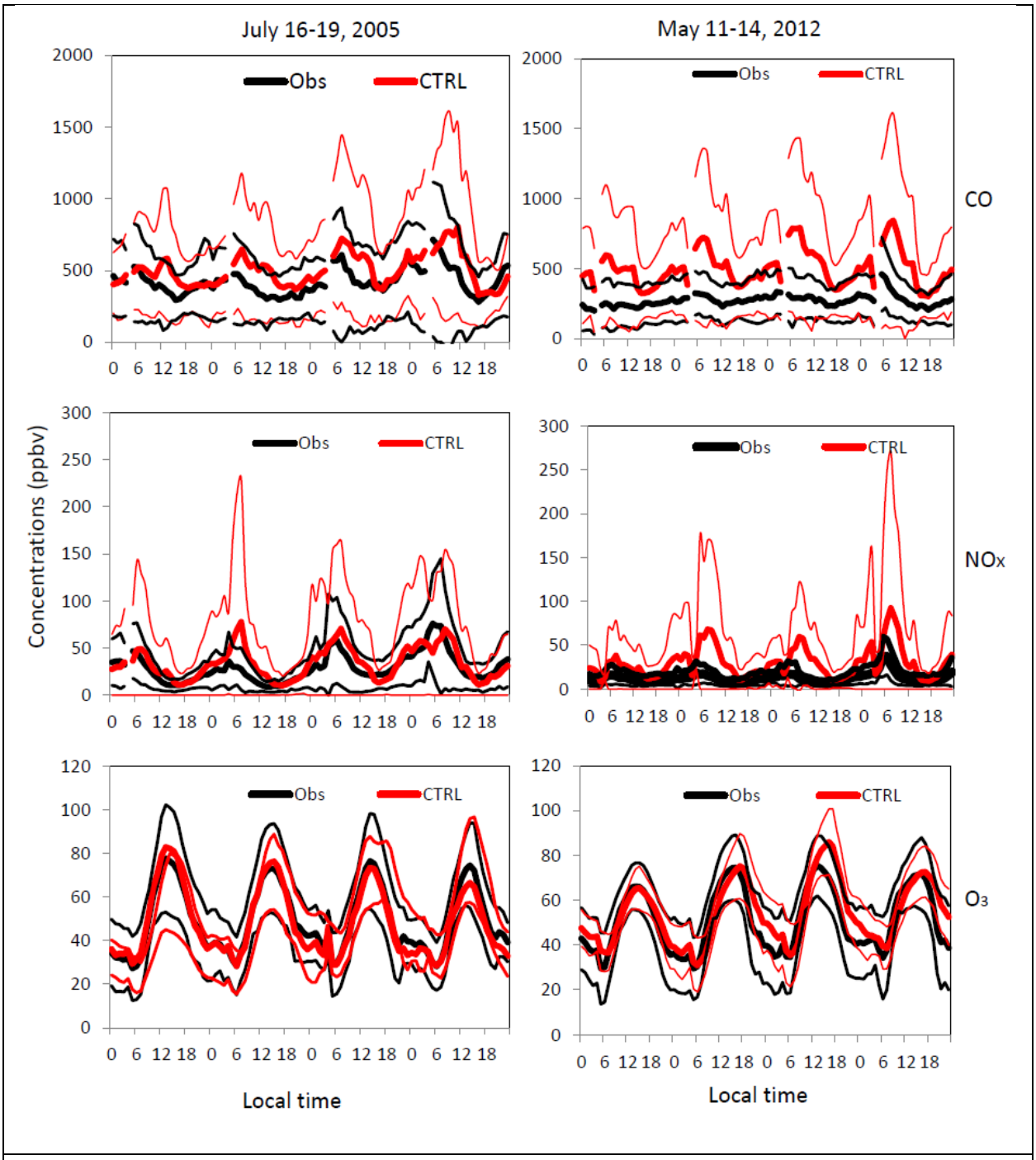

Figure 3: The comparisons of CO, NOx, and O_3 concentrations between observations (bold black) and simulations (bold red) in Domain 4. There are 23 sites for NOx, 20 sites for CO, and 65 sites for O_3 observations during the study time periods. The locations are shown in Figure 1b. The variation ranges of simulation and observation are correspondently labeled by thin-red-line and thin-black-line, respectively. Missing observation time (4:00 local time) is masked in the figure. CTRL represents WRF-Chem control run.

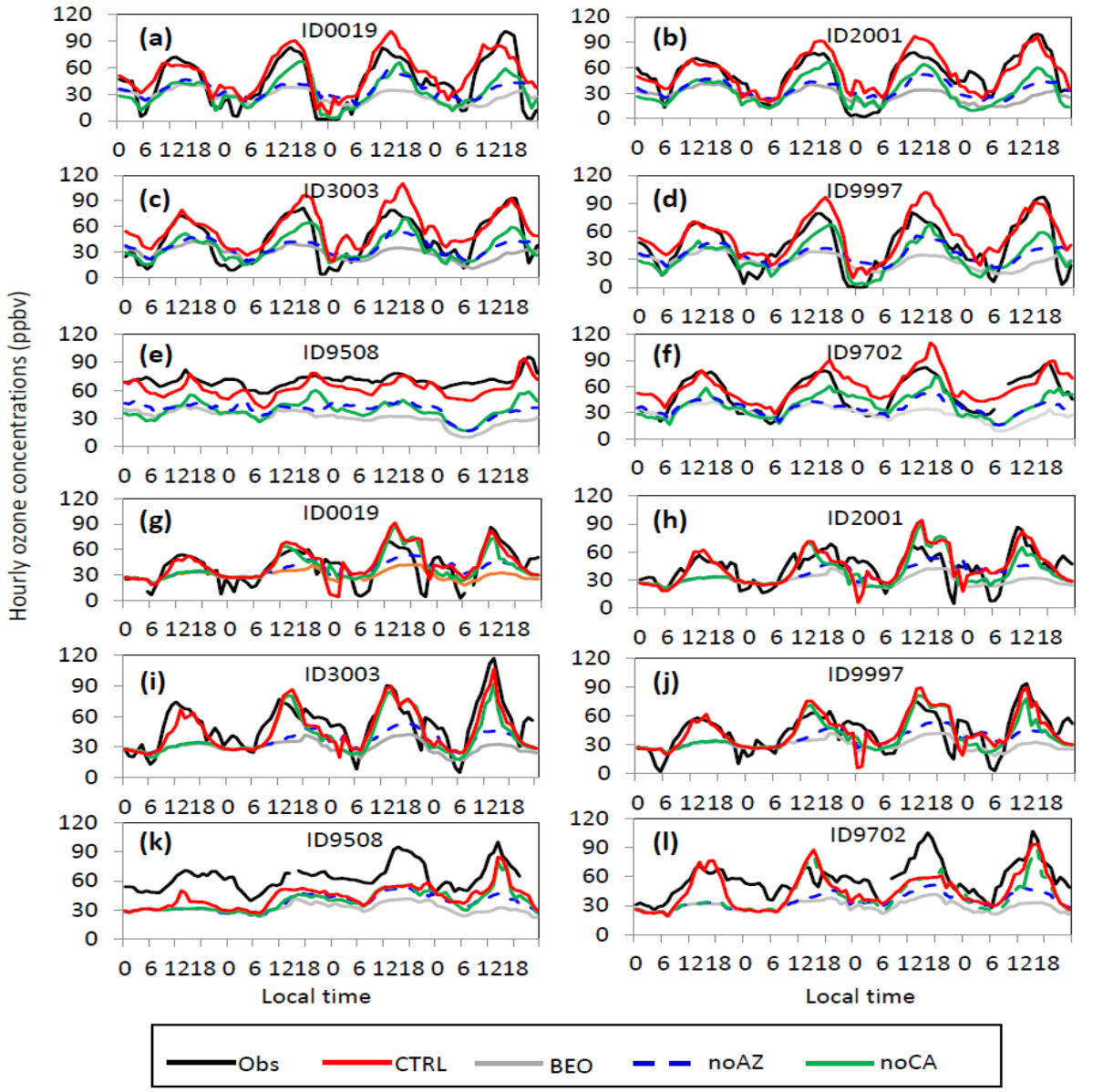

Figure 4: Relative contributions of different emission scenarios to [O_3] at observation sites in Phoenix metropolitan area and surrounding rural areas. The dates are May 11-14, 2012 (Figure 4a-4f) and July 16-19, 2005(Figures 4g-4l). Idxxxx corresponds to the EPA AIRS site number in Maricopa County, Arizona. Black line indicates the [O_3] observation. Red line represents the simulated [O_3] for the CTRL run. Blue line shows the [O_3] for the noAZ run. Green line displays the [O_3] for the noCA run. Gray line is the [O_3] for the BEO run.

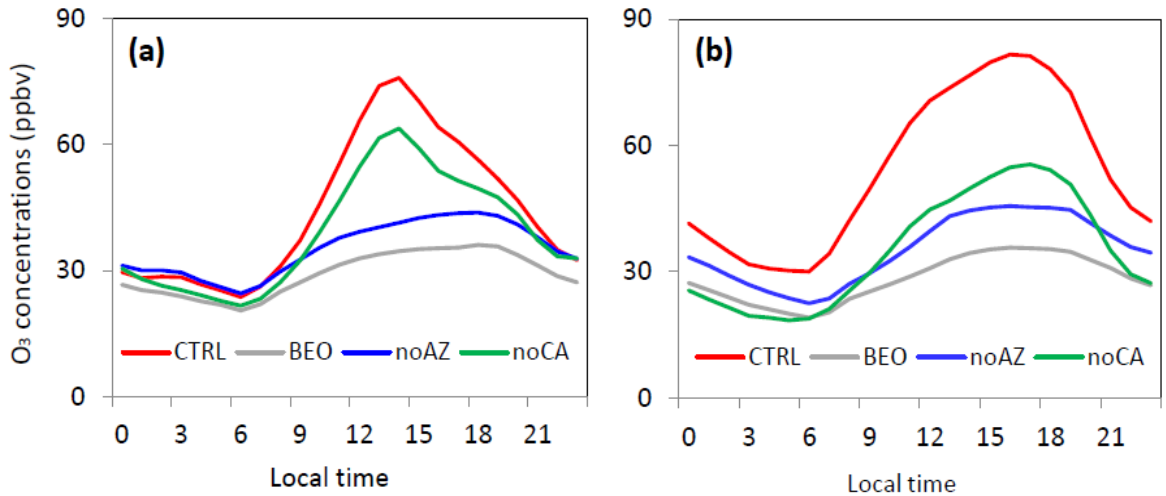

Figure 5: Simulated diurnal variations of [O_3] at Phoenix urban setting for different emission scenarios: (a) average from July 16-19, 2005, and (b) average from May 11-14, 2012.

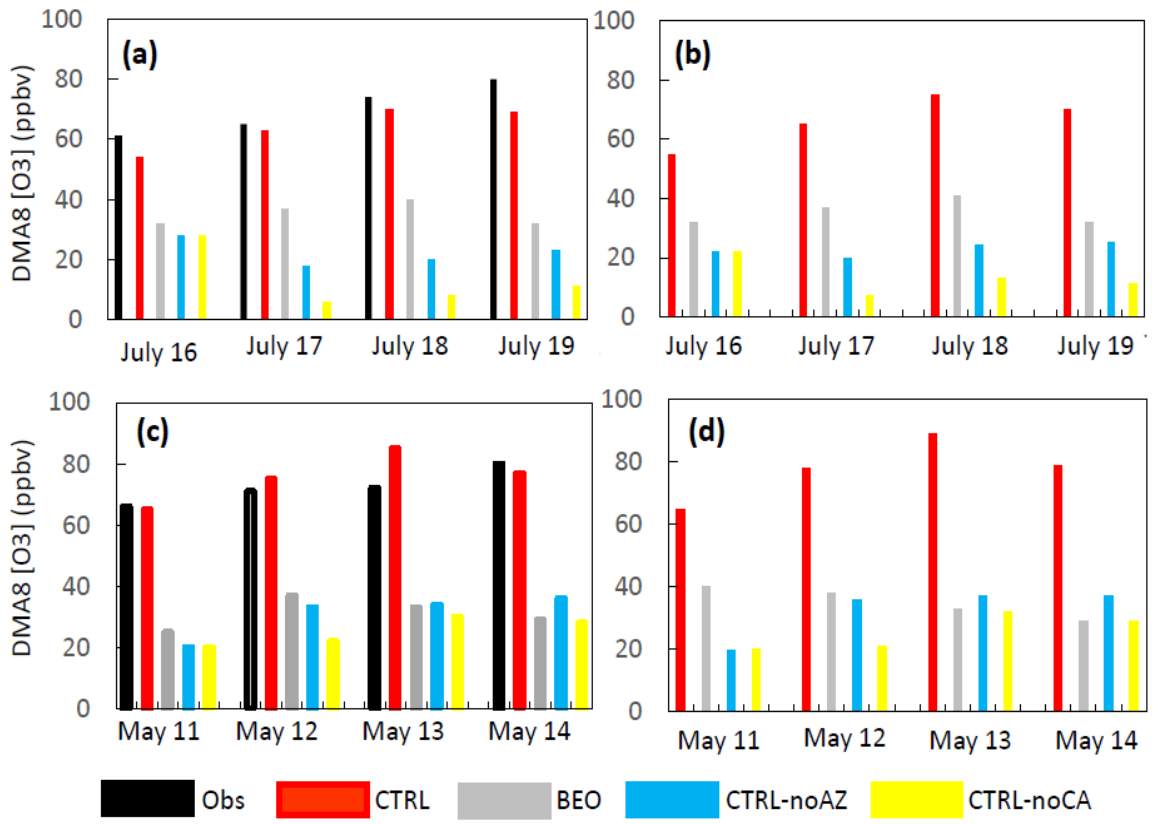

Figure 6: Mean DMA8 [O_3] in Phoenix metropolitan area from observation (Obs), simulation from CTRL runs (CTRL), BEO runs (BEO), and the relative contributions of different emission sources. CTRL-noAZ represents the modeled DMA8 [O_3] differences between CTRL run and noAZ run. CTRL-noCA displays the modeled DMA8 [O_3] differences between CTRL run and noCA run. Observation sites show in Figure 1b. (a) DMA8 {O3] at observation sites for July 16-19, 2005, (b) the same as (a) but for that averaged from Phoenix urban grid cells. (c) and (d), the same as (a) and (b) but for the case of May 11-14, 2012.

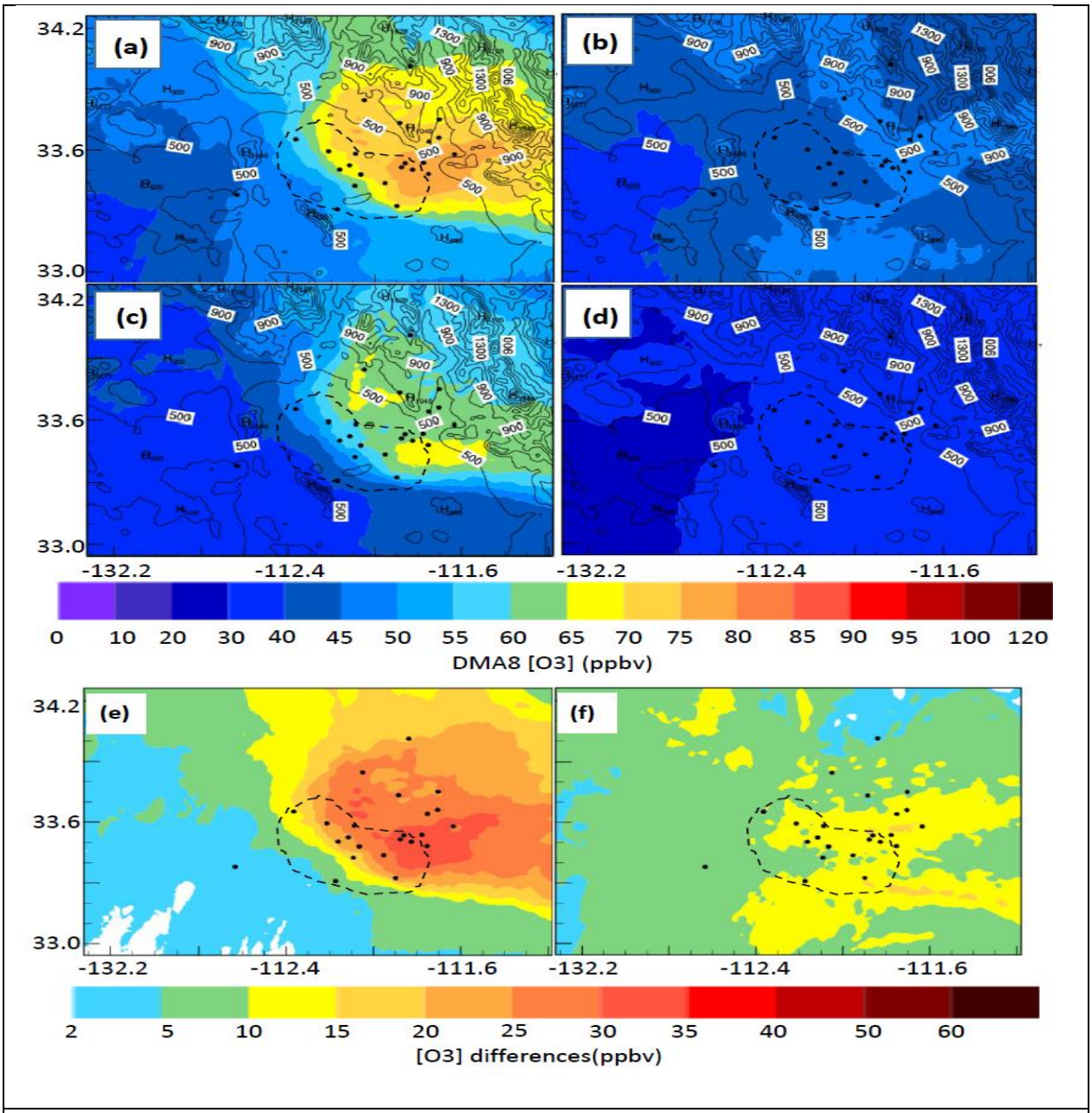

Figure 7: DMA8 [O3] spatial distributions in Greater Phoenix and surround areas on July 19, 2005: (a) CTRL, (b), noAZ, (c) noCA, (d) BEO, (e) CTRL-noAZ, and (f) CTRL-noCA. Contours represent terrain elevations. Dots shows O3 observation site. Circle indicates the approximate location of Phoenix urban area.

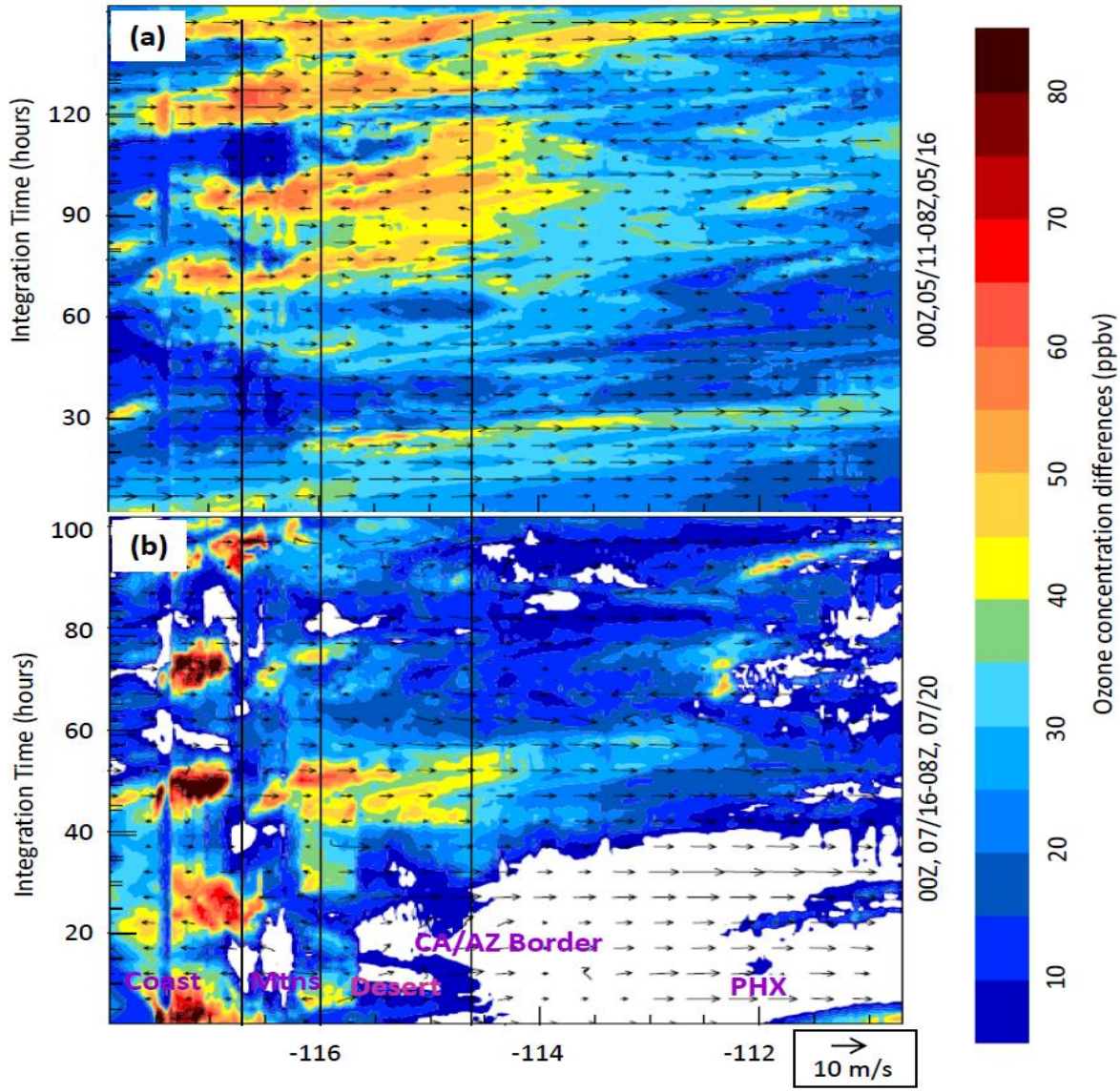

Figure 8: Hovmoller diagram of [O_3] differences (CTRL minus noCA) at 13th vertical model layer (about 1100-m agl) along the cross-section B'B shown in Figure 1b for July case (top) and May case (bottom). Approximate locations of Phoenix (PHX), desert, mountains (Mnts), and coast are also labeled in Figure 7. The integrating is counted from 00Z, May 10, 2012, and 00Z, July 15, 2005, respectively.

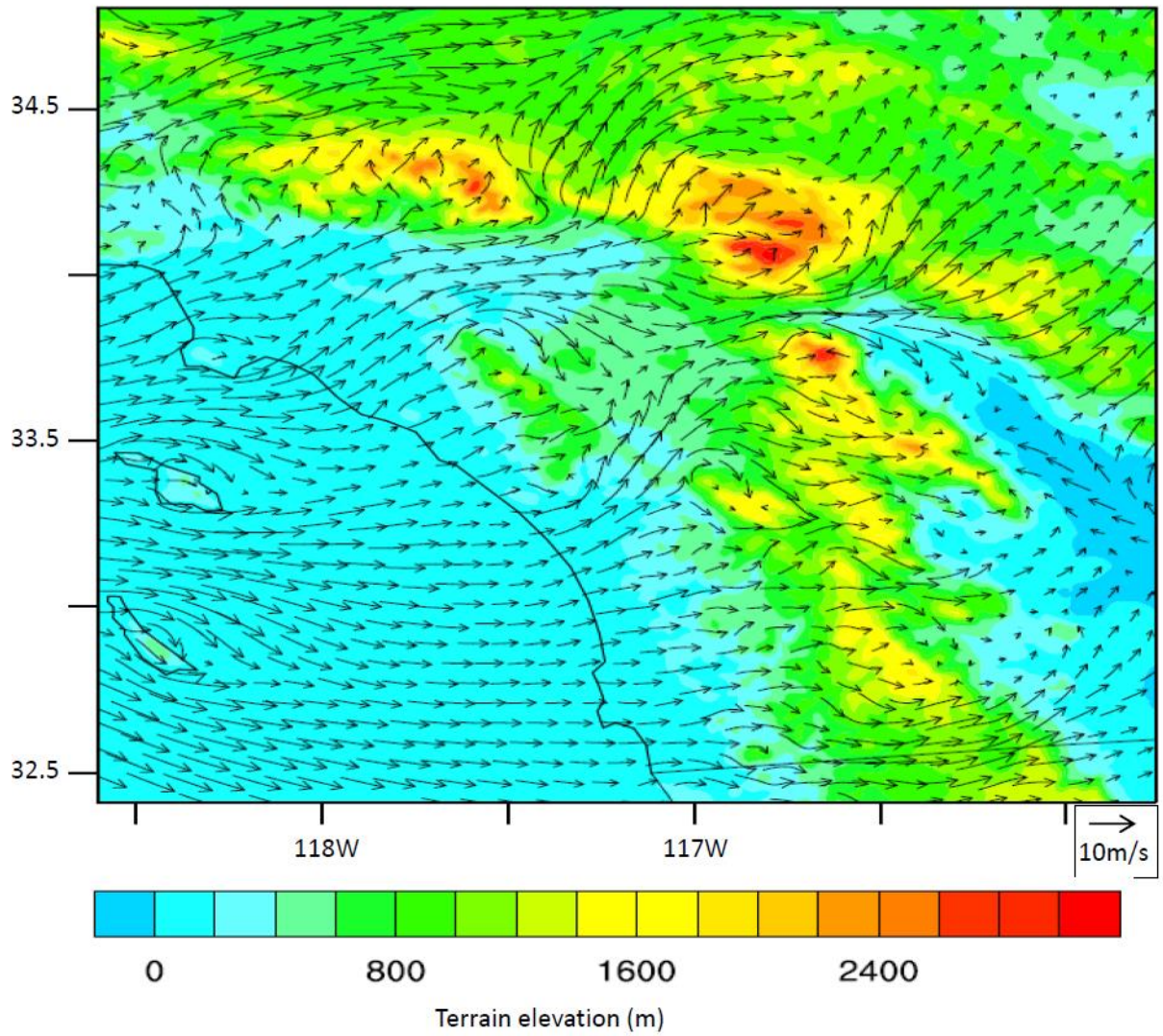

Figure 9: Wind vector field at 40-m above surface layer in southern California coastal area.

Data are averaged from 20Z to 02Z, July 16-20, 2005.

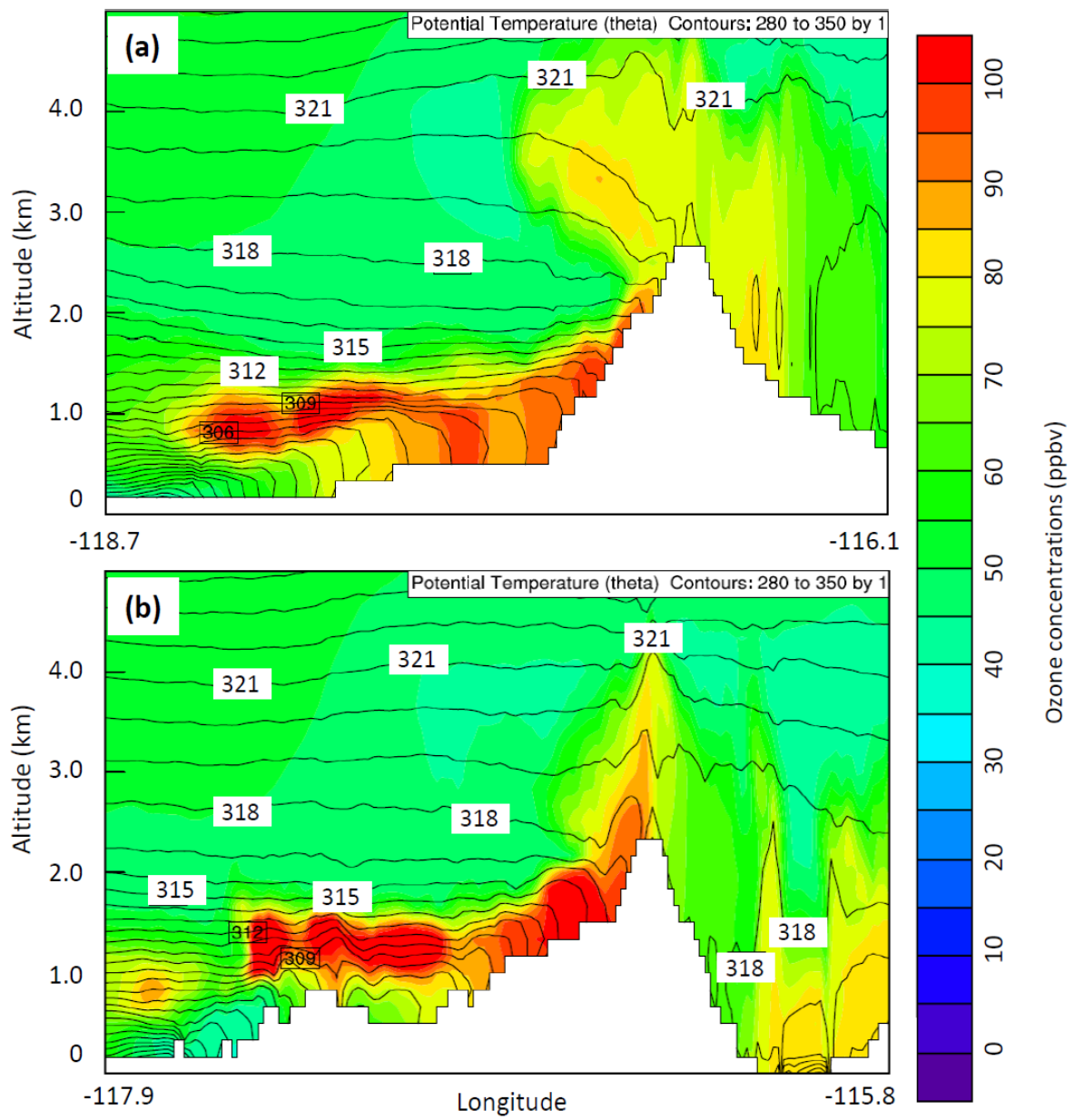

Figure 10: Vertical distributions of ozone along cross-section A'A (Figure 9a) and B'B (Figure 9b) shown in Figure 1b at 22Z of July, 17, 2005. The contours are potential temperature starting at 280-K with 1-K interval.

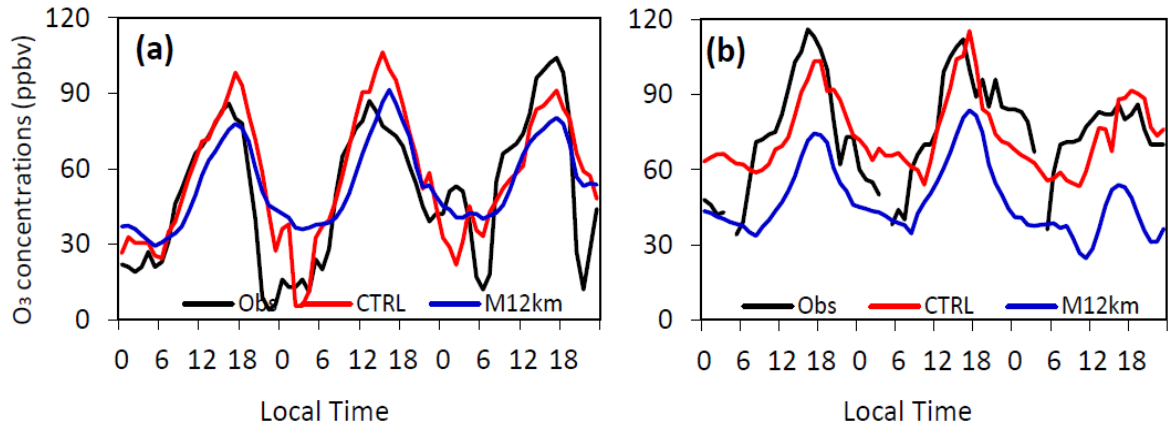

Figure 11: Ground-level ozone concentration comparisons between observations and simulations at (a) Banning Airport (ID0650012, 33.92077°, -116.85841°) located in the San Gorgonio Pass and (b) Crestline (ID060710005, 34.24313°,-117.2723°) near Cajon Pass from July 17-19, 2005. Obs indicates the observation. CTRL represents the simulations from CTRL run and M12km is the model simulations at 12-km resolution.

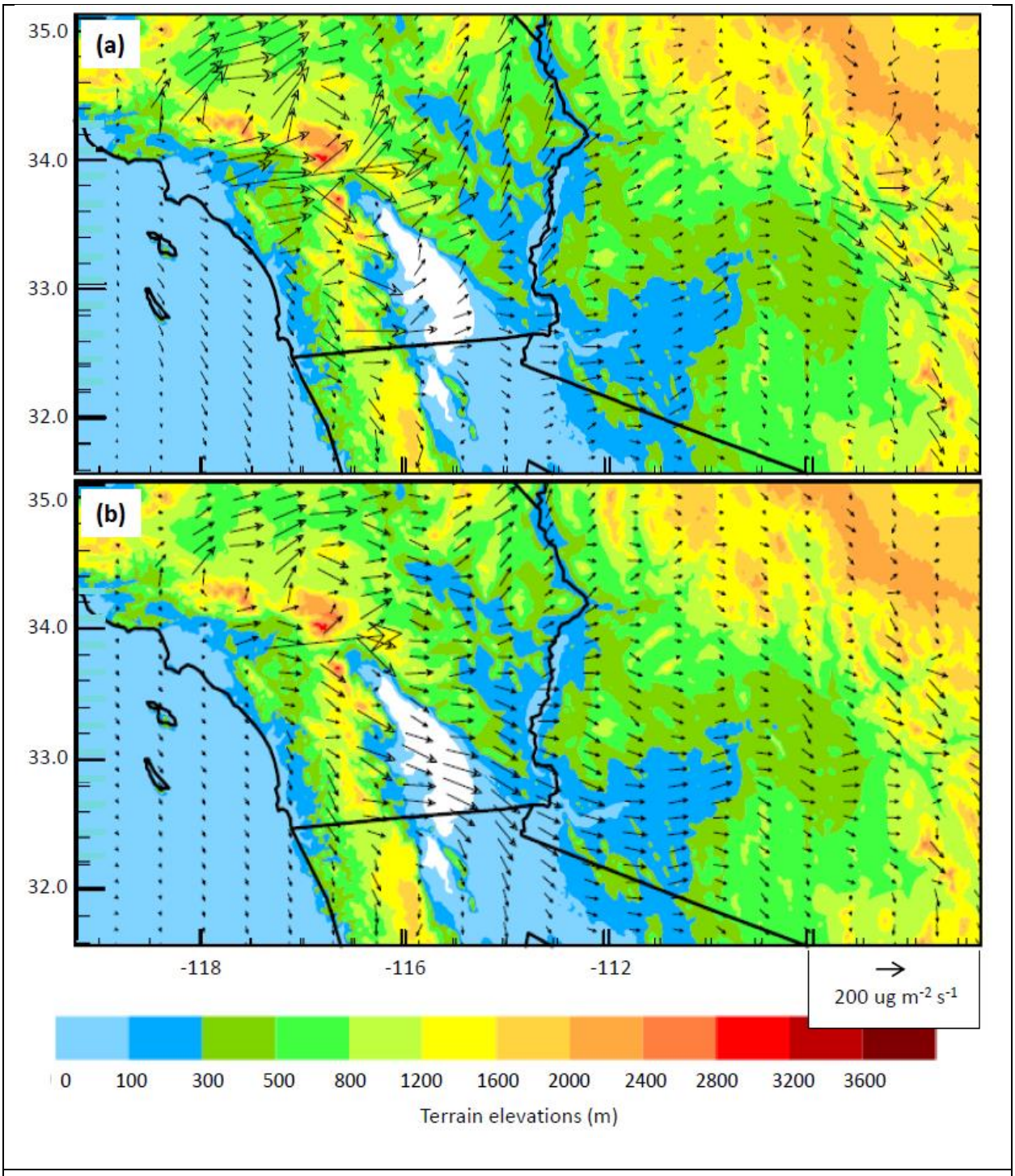

Figure 12: Integrated fluxes of ozone differences (CTRL-noCA) from surface to 1400 m above ground-level: (a) average from 18Z to 02Z, July 16 to July 20, 2005, and (b) average from 03Z to 17Z, July 16 to July 20, 2005.

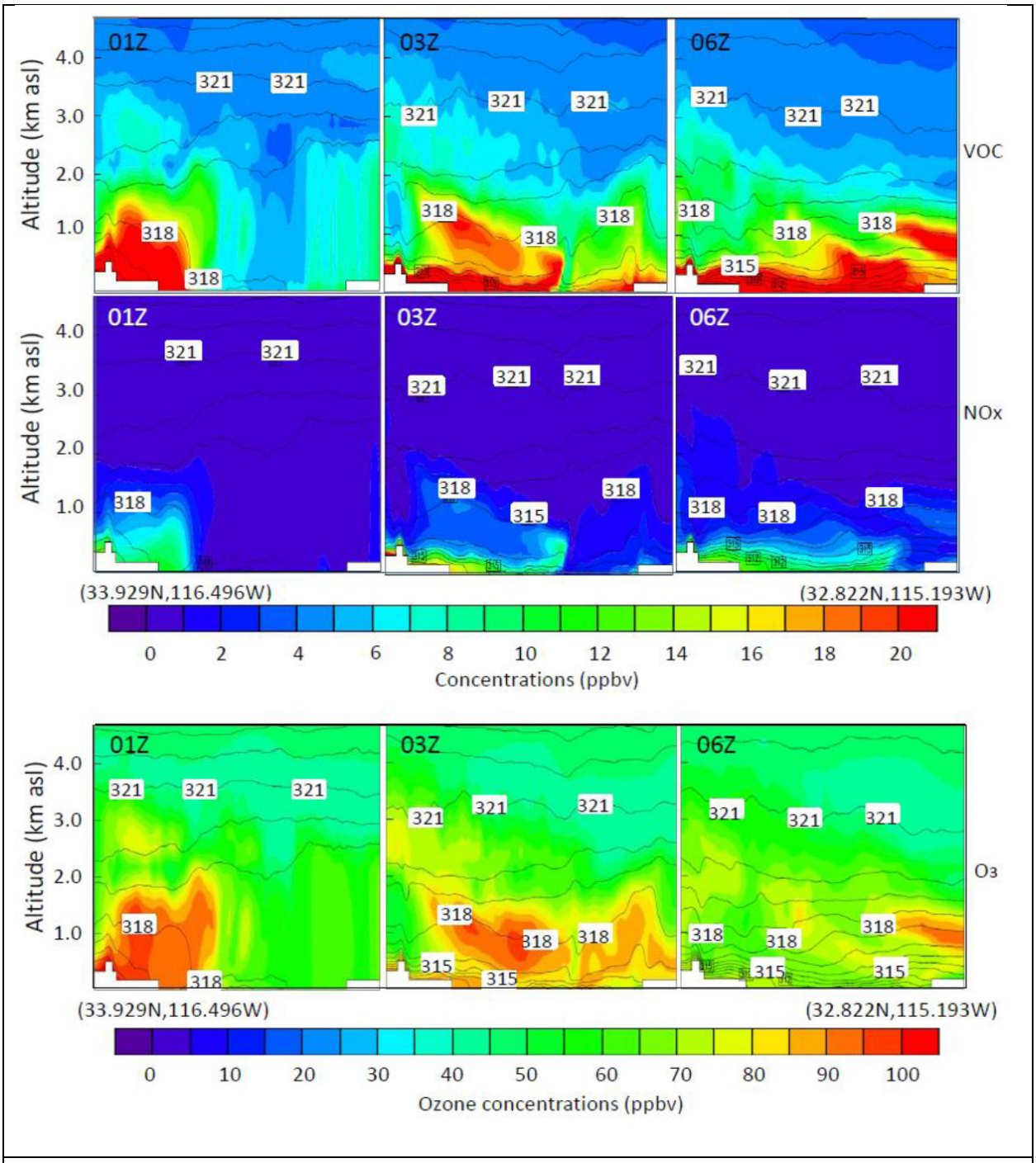

Figure 13: The vertical distribution of VOC (top), NOx (middle), and O_3 (bottom) along the cross-section D'D (shown in Figure 1b) in Salton Sea Basin at 01Z, 03Z, and 06Z, July 18, 2005. Contours are potential temperature with 1-K interval.

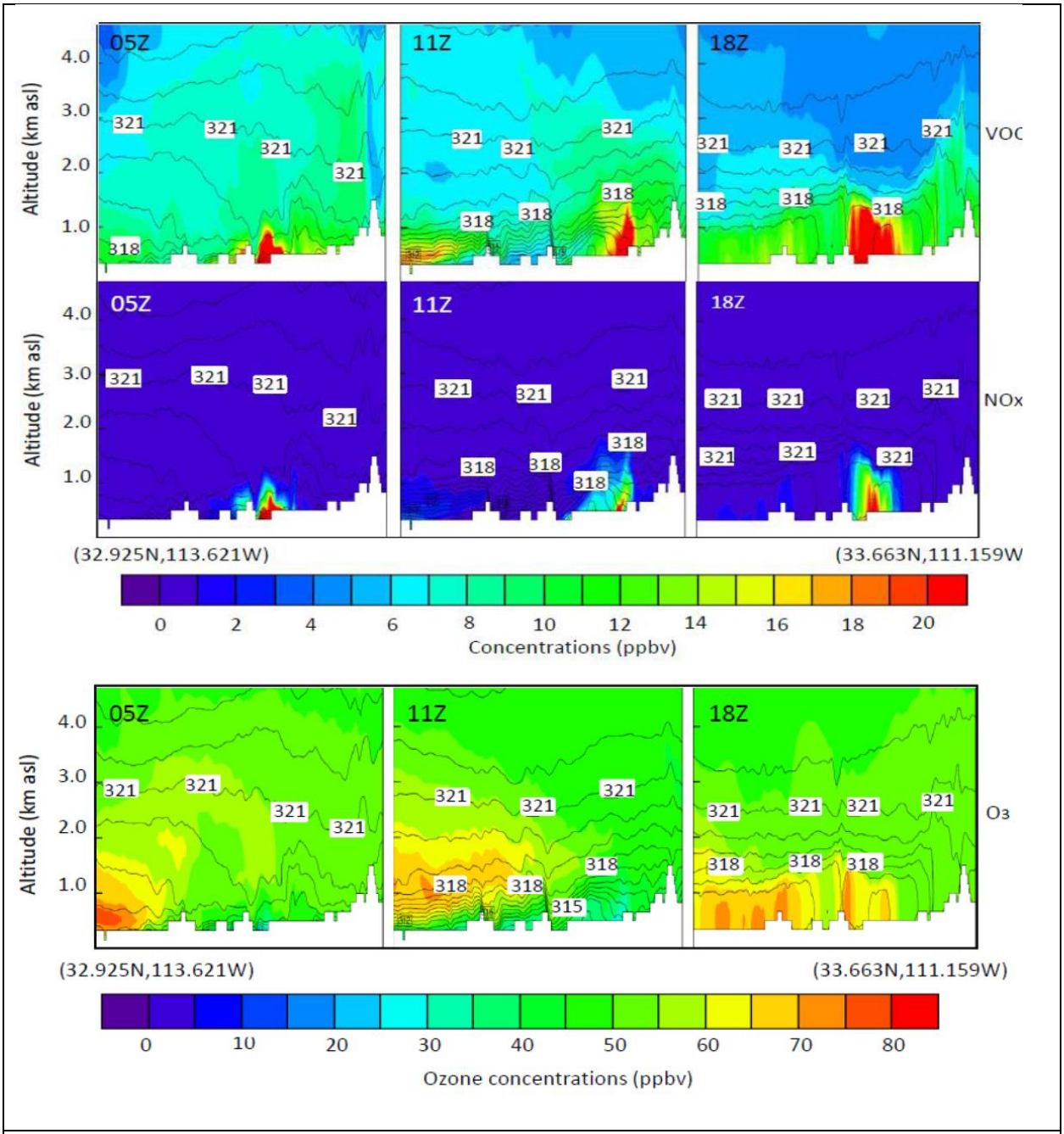

Figure 14: The vertical distribution of VOC (top), NOx (middle), and O_3 (bottom) along the cross-section D'D (shown in Figure 1b) in Gila River Basin, Arizona at 05Z, 11Z, and 18Z, July 18, 2005. Contours are potential temperature with 1-K interval.